VYSOKÉ UČENÍ TECHNICKÉ V BRNĚ

Fakulta chemická

Ústav fyzikální a spotřební chemie

RNDr. František Krčma, Ph.D.

KINETIC PROCESSES IN NITROGEN POST-DISCHARGE PLASMAS

KINETICKÉ PROCESY V DOHASÍNAJÍCÍM DUSÍKOVÉM PLAZMATU

SHORT VERSION OF HABILITATION THESIS

VUTIUM

BRNO 2004

KEY WORDS

Afterglow, atomic recombination, CN spectra emission, collisional excitation energy transfer, DC discharge, decaying plasma, halogenated hydrocarbons, hydrocarbon traces, kinetic processes, liquid nitrogen temperature, low-temperature plasmas, microwave discharge, molecular nitrogen, nitrogen pink afterglow, nitrogen spectra emission, optical emission spectroscopy, polymers disintegration, post-discharge, pure nitrogen, quenching, step-vise ionization.

KLÍČOVÁ SLOVA

Atomární rekombinace, čistý dusík, dohasínající plazma, dusíkové „pink afterglow“, emise dusíkových spekter, emise spekter CN radikálu, halogenované uhlovodíky, kinetické procesy, mikrovlnný výboj, molekulární dusík, nízkoteplotní plazma, optická emisní spektroskopie, přenos excitační energie během srážek, „quenching“, rozpad polymerů, rozpadající se plazma, stejnosměrný výboj, step-vise ionizace, teplota kapalného dusíku, uhlovodíkové stopové příměsi.

Habilitation work is stored at the Institute of Physical and Applied Chemistry at Faculty of Chemistry of Brno University of Technology, Purkyňova 118, Brno.

Habilitační práce je uložena na Ústavu fyzikální a spotřební chemie Fakulty chemické Vysokého učení technického v Brně, Purkyňova 118, Brno.

ISBN 80-214-2572-5
ISSN 1213-418X

ABSTRACT

The work presents the results obtained during the spectroscopic observations of DC and microwave post-discharges of the pure nitrogen plasmas and nitrogen plasmas containing traces of hydrocarbons and halogenated hydrocarbons. The plasmas have been studied by the emission spectroscopy of three nitrogen and two CN spectral systems.

The $N_2(B\,^3\Pi_g)$, $N_2(C\,^3\Pi_u)$ and $N_2^+(B\,^2\Sigma_u^+)$ vibrational distributions have been studied as a function of decay time at wall temperatures in the interval of 77 – 300 K in the pure nitrogen DC afterglow. The quenching of the nitrogen pink afterglow by the hydrocarbon traces was directly studied and it was shown that the maximum of the pink afterglow intensity is decreasing proportionally to the increase of the methane concentration. The position of the maximum emission is also linearly shifted to the later decay times. The vibrational distributions of $N_2(B\,^3\Pi_g)$ and CN ($A\,^2\Pi$)) states have been studied as a function of the methane concentration at six selected decay times at wall temperatures of 77 K and 300 K. The influence of hydrocarbon presence on the other observed spectral systems was studied at the same experimental conditions through the selected band, only, due to the strong overlapping of these systems. The strong CN violet system emission was measured at higher hydrocarbon concentrations, especially at 77 K wall temperature.

Due to the very high sensitivity to the methane presence a new method of hydrocarbon traces detection in pure nitrogen was proposed and further developed. For its application in determination of the polymer material destruction the influence of various partially or fully halogenated hydrocarbons was verified. The detection limit of this method is about 0.05 ppm of carbon atoms in the pure nitrogen. The direct measurements of the destruction of polyethylene and polypropylene samples were presented.

On the base of the experimental results, the appropriate kinetic model of the plasma excited in pure nitrogen and in nitrogen with carbon containing traces was designed. The specific state-to-state energy transfer reactions among the studied states are presented.

ABSTRAKT

Práce přináší výsledky získané během spektroskopických pozorování dohasínajícího stejnosměrného a mikrovlnného plazmatu buzeného v čistém dusíku a v jeho směsích s uhlík obsahujícími stopovými příměsemi. Plazma bylo studováno emisní spektroskopií tří spektrálních systémů dusíku a dvou systémů radikálu CN.

Vibrační rozdělení stavů $N_2(B\,^3\Pi_g)$, $N_2(C\,^3\Pi_u)$ a $N_2^+(B\,^2\Sigma_u^+)$ bylo měřeno v čistém dusíku v závislosti na čase rozpadu stejnosměrného plazmatu při teplotě stěny v rozmezí 77 – 300 K. Podrobně bylo proměřeno zhášení tzv. „pink afterglow“ vlivem přítomnosti uhlovodíků v plazmatu, přičemž se ukázalo, že intenzita maximálního vyzařování klesá přímo úměrně s růstem koncentrace uhlíku ve výboji a současně se posunuje maximum vyzařování k pozdějším časům v rozpadu. V závislosti na koncentraci metanu byly studovány změny vibračních populací stavů $N_2(B\,^3\Pi_g)$ a CN ($A\,^2\Pi$) v šesti vybraných časech rozpadu při teplotách 77 a 300 K. Vliv příměsi na ostatní spektrální systémy byl studován za stejných podmínek pomocí intenzit vybraných spektrálních pásů, neboť vzájemný překryv těchto systémů znemožňuje stanovení vibračních populací příslušných stavů. Byla pozorovány silná emise fialového systému CN, zejména za snížené teploty.

Na základě vysoké citlivosti dohasínajícího dusíkového plazmatu na přítomnost uhlíku jsme navrhli a vyvinuli novou metodu pro stanovování rozpadu polymerních materiálů. Její detekční limit byl stanoven na cca 0,05 ppm uhlíkových atomů v čistém dusíku. Metoda byla pokusně použita pro měření rozpadu polyetylénu a polypropylénu.

Na základě experimentálních výsledků byl vytvořen model kinetických procesů probíhajících v dohasínajícím plazmatu v čistém dusíku obsahujícím stopové příměsi uhlovodíků a současně byly stanoveny konkrétní reakce mezi jednotlivými excitovanými stavy.

About author

Name: František,
Surname: Krčma,
Title: RNDr. Ph.D.
Born: 23. March 1968
Affiliation: Brno University of Technology,
Faculty of Chemistry, Purkyňova 118, 612 00 Brno
Tel.: * 420 541 149 407, **Fax:** * 420 541 211 697,
e-mail: krcma@fch.vutbr.cz, **http:** www.fch.vutbr.cz/~krcma/
Position: Assisted professor

Graduation: **1991:** RNDr. at Faculty of Science, Masaryk University Brno, physical electronics, Diploma Thesis *Study of Physical Condition Influence on the Nitrogen Afterglow*, supervisor Assoc. Prof. A. Tálský.
1995: PhD. at Faculty of Science, Masaryk University Brno, plasma physics, PhD. Thesis *Spectroscopic Studies of the Methane Traces Influence on the Nitrogen Afterglow,* supervisor Assoc. Prof. A. Tálský.

Employment: **1986 – 1991:** Student at Faculty of Science, MU Brno, physical electronics
1991 – 1995: PhD. student at Faculty of Science, MU Brno, plasma physics
1996 Researcher at Institute of Plasma Physics, Czech Academy of Science, Prague
Since 1997: Assisted professor at Faculty of Chemistry, BUT

Scientific activity abroad: Université Paris-Sud, France (Prof. A. Ricard, 1994 - 5 months), École Nationale Superiére du Chimie de Paris, France (Prof. J. Amouroux, 1995-1996 - 6 months), 3 short study stays at both these universities.

Research activities: Optical diagnostics of the low-temperature and thermal plasmas and afterglows, chemical kinetics of plasmas created in nitrogen and nitrogen mixtures, dominantly with methane, numerical simulation of the diatomic molecular spectra, photographic a video documentation of various discharge plasmas.

Teaching 2003: Lectures from Physical chemistry – Applied Quantum mechanics (Mgr. course), practical and theoretical works from Physics (Bc course), practical works from Plasmachemistry, Photographic chemistry and Image engineering (all Mgr. courses). Since 2000 supervisor of 14 Mgr. Thesis, since 2002 supervisor of 5 PhD. Thesis.

Publishing: Author and co-author of 1 monograph, 14 scientific papers, 65 conference contributions, 4 invited lectures at international conferences, 2 text books, 1 database.

Grants:

- Applicant of the grant project *Etude des Réactions Cinétiques dans la Post-Décharge d'un Plasma Ar–N_2–CH_4*, Robert Schuman Foundation, France (1995-1996).
- Applicant of grant project *Study of the Processes in Plasma Created in Ar-N_2-CH_4 Gas Mixture,* GA AS ČR C104 3601 (1996).
- Applicant of the post-doctoral grant project *Study of the Processes in Post-discharge Plasma Created in Pure Nitrogen with Chloro- and Fluoro-Carbons and Their Application in Determination of the Plastic Materials Degradation*, GAČR 202/98/P258 (1998-2001).
- Joint-applicant of the grant project *Surface Activation of Synthetic Polymer Materials in Non-Isothermic Low Temperature Plasma*, GAČR 104/99/0307 (1999-2001).
- Joint-Applicant of the doctoral grant project, Advanced Topics in Physics and Chemistry of Plasmas, GAČR 202/03/H162 (2003-2007).
- Applicant and joint-applicant of 15 grant projects of Czech Ministry of Education (FRVŠ)

CONTENTS

1 INTRODUCTION

Nitrogen post-discharges have been the subject of many studies for more than 50 years. These studies focus not only on the knowledge of the basic processes but also on their practical applications. The research in Europe is concentrated in several laboratories, dominantly in France (Paris, Lille, Toulouse, Grenoble, Pau). Electric probe measurements in nitrogen plasmas are widely carried out in Greifswald (Germany), laser induced fluorescence is used in Bari (Italy). Kinetic models of processes in nitrogen post-discharges are developed in Lisbon (Portugal) and in Prague (Czech Republic). Besides the European laboratories, groups in the USA, Japan, Canada and some other countries include nitrogen post-discharge among the subjects studied.

Other laboratories use the nitrogen plasmas for various technological applications. Neutral molecular nitrogen forms dominantly diatomic molecules, which can form 102 different electronic states with many different vibrational states, each of them with huge number of rotational states. Due to this fact, molecular nitrogen forms one of the most complicated diatomic molecular systems. At usual thermodynamic conditions the few lowest vibrational and rotational states of the electronic ground state can be observed. On the other hand, under the plasmatic conditions all the electronic states can be observed. These states are created at the Earth conditions dominantly by various electrical discharges. The excited states are produced dominantly by collisions of heavy particles with electrons under the discharge conditions. Besides these states, atoms and molecular ions are produced, both also in the excited states.

After the active discharge is switched off, many processes leading to laboratory thermodynamic equilibrium (about 300 K) can be observed. This period is known as post-discharge or afterglow. During the first few microseconds of the post-discharge period, the quasi-neutral active plasma, due to the fast electron-ion recombination, is transformed into a neutral form with high-excited molecular gas containing a significant amount of atoms. During this period, which takes a long time (from several minutes up to several hours), the dominant processes are the atomic and molecular collisions and light emission. These processes give information about the structure of molecules, their excitations, energy transfer reactions, etc. Knowledge of these processes can help in their practical applications.

Many different plasmachemical methods and processes are used in the common industrial practice. One of the most widely used methods is the plasmachemical nitridation of surfaces and plasmachemical deposition of special thin films, such as titanium nitride. In these applications, the discharge created in an Ar–N_2 mixture is used and very hard surface layers are created for many different purposes. Use of active discharges in these applications brings some problems. Recently it was demonstrated that during the thin film preparation in an active discharge the surface is sputtered by bombardment with energetic heavy particles (these heavy particles are usually ions). This negative effect can be eliminated if a microwave discharge is used (in this type of discharge the ion energy is not so high as in the DC discharge). It was shown that for some plasmachemical processes it is better to use a post-discharge instead of the active discharge [3].

In the post-discharge there are only a few ions due to the very high rate of the electron-ion recombination. On the other hand, in the post-discharge there are many atoms as well as many electronically and vibrationally excited molecules. Energy of these particles is sufficient for many plasmachemical processes. Due to these facts the afterglow conditions can be much better for technological applications.

During the studies (experimental studies as well as studies based on computer simulations) of plasmachemical processes it was demonstrated that many processes observed in plasmas are very sensitive to the plasma conditions and plasma composition. Therefore, it is necessary to study such processes and their practical applications. There is also a high probability of finding new processes that could be further applied in industry. Some of the results can be used in other scientific branches, too.

Pure nitrogen and its afterglow were subject of several hundred studies. These studies provide a lot of information about kinetic processes and energy transfer channels and reactions. Presence of some

impurities in pure nitrogen can significantly change these kinetic processes. This effect is well known for the carbon containing impurities that are often present at practical applications.

The simplest molecule containing carbon is CH_4. Up to now the greatest deal of all studies on this mixture has been focused on the higher methane concentrations (higher than 0.01 % CH_4 in pure nitrogen), although it is known for many years that significant changes in the emission spectra can be observed at hydrocarbon concentrations many orders lower. These impurities are usually presented as impurities in the used gas or desorbed molecules from the plasma reactor wall. Changes in the spectra are more significant in the afterglow, especially at lower wall temperatures. It was proved that a small methane addition (0.01 – 300 ppm) has a great influence on molecular nitrogen dissociation in an active discharge as well as on strong depopulation of highly excited molecular states in the afterglow.

For experimental studies of selected excited states only optical spectroscopy can be used, because the other plasma diagnostic methods (except for a relatively rare EPR plasma spectroscopy) could not give any information about neutral molecules. The emission spectroscopy is the best method because it allows the time-resolved measurements without any technical difficulties. A base for the presented study was also partly obtained from the huge bibliography. There are also results obtained by the other techniques as the electrical probes and absorption spectroscopy.

2 HISTORY OF THE STUDIES

The first experiments were carried out during the second half of 1980s. The subject of the experiments was the study of pure nitrogen afterglow at ambient and low (liquid nitrogen) temperatures using microwave discharge as a plasma source. Two different for us unknown spectral systems were observed during the afterglow besides the well-known nitrogen first (N_2 ($B\ ^3\Pi_g$) $\rightarrow$ N_2 ($A\ ^3\Sigma_u^+$)) and second (N_2 ($C\ ^3\Pi_u$) $\rightarrow$ N_2 ($B\ ^3\Pi_g$)) positive and first negative (N_2^+ ($B\ ^2\Sigma_u^+$) $\rightarrow$ N_2^+ ($X\ ^2\Sigma_g^+$)) spectral bands. The first of these systems shows the same structure as the nitrogen first positive system and using the molecular calculations it was identified as transitions from the vibrational levels lying over the predissociation limit of the N_2 ($B\ ^3\Pi_g$) state. This calculation was later confirmed using the scientific sources that were inaccessible before the 1989 revolution. These spectral transitions are not usually observed under laboratory conditions but they are common in the radiation of upper atmosphere in Corona Borealis.

The identification of the other unknown spectral system was more complicated. This system could be observed in our experiment at ambient temperature but when the temperature decreased the intensity of this system became dominant in the spectrum. Structure of its bands was for us unknown and it did not correspond to any system in the spectral tables. In this situation the colleagues from Prof. Ricard's group in France helped us (a co-operation established in the 1960s has been renewed). They identified these bands as CN violet (CN ($B\ ^2\Sigma^+$) $\rightarrow$ CN ($X\ ^2\Sigma^+$)) spectral system and they gave us the numerical simulation of these bands under our conditions (low temperature).

It was necessary to solve the problem why the CN spectrum can be observed in pure nitrogen post-discharge. Due to the fact that the nitrogen of high purity (99.9999 %) was used the carbon source had to be present in the experimental device. Initially the fittings using vacuum grease were replaced and the whole device was completely cleaned. Now the entire experimental device was glass (Pyrex and Quartz) made coupled with two connection lines from polyethylene. This improvement caused decrease of the CN bands intensity but they were still dominant in the spectrum at the decreased temperature. Thus glass and stainless steel tubes replaced the polyethylene with no carbon containing materials. In the spectra recorded after this full reconstruction of the experimental set-up the CN bands were remarkable with very low intensity at low temperature only. The idea of unusual sensitivity of the nitrogen afterglow to carbon traces was proposed because at the preceding step only two polyethylene tubes of total 3m length were used in the experimental device.

The next studies were focused on the verification of what the pure nitrogen afterglow containing carbon traces in concentrations of ppm looks like. Methane was chosen as the source of carbon. The

experimental results showed the possibility to detect carbon in concentrations higher then 0.01 ppm. This high sensitivity evoked the search of potential application. The first idea proposed in Appendix 1 was to apply the high sensitivity in the detection of polymeric materials disintegration. During my study stay in 1994 at Laboratoire de Physique des Gas et Plasmas at Universite Paris-Sud in Orsay (Prof. Ricard) I have had the opportunity to continue with this research using the DC post-discharge at ambient temperature. These experiments confirmed the previous results obtained from the microwave afterglow.

During the next period of the experimental research, a post-doctoral stay at Institute of Plasma Physics at Czech Academy of Science in Prague I have constructed a new experimental device using the DC afterglow. The studies were focused on the pure nitrogen afterglow and nitrogen containing methane traces at temperatures between liquid nitrogen and ambient temperature. All the results again confirmed the unusual sensitivity of the high nitrogen afterglow to the carbon traces. The experiments with methane were followed by the confirmation of the possibility to measure the polymer disintegration by the proposed method.

The last experimental period up to now has been orientated towards the verification if the traces of other hydrocarbons, also halogenated, show the same effect on the nitrogen afterglow. The focus on this group of hydrocarbons was evoked from the composition of some special plastic materials, such as Teflon. A new experimental set-up was constructed again at the Department of Physical Electronic at Masaryk University of Brno using the DC post-discharge. The experiments fully confirmed all our previous ideas. The simplified detection device was proposed on this huge experimental basis and tested. At present, its final version is under construction.

Simultaneously with the experimental works, theoretical study of the kinetic processes resulting in the observed phenomena was realized. The details are given in the later part of this work.

3 EXPERIMENTAL DEVICES

The post-discharge is a process that is running for a relatively long time up to many minutes or hours. It is a general knowledge that after the street lamps are switched off, some visible radiation can be observed for a long time, up to one minute. This is the post-discharge, which is the subject of this study. There are two possibilities how to study this discharge period. The first one is called stationary regime. It means that the time resolution is given using the changing delay between switching off and measurement. To obtain the results with time resolution in the order of milliseconds it is necessary to repeat each measurement many times. It is not too easy when optical emission spectroscopy is used. The flowing afterglow is the other possible configuration. The gas is flowing through the active discharge region where the molecules are ionized, dissociated and excited and then they are transferred by the gas flow through the post-discharge tube. Thus the switch-off point is at the point where the gas (plasma) is leaving the space of an active discharge. The scheme of one of the devices used for this study is presented in Fig. 1. The gas velocity gives the time along the post-discharge, only, and the time evolution of the afterglow is characterized by the space position from the end of an active discharge. This configuration allows the time resolution up to the order of microseconds but usually for the study of kinetic processes during the post-discharge the millisecond order is used.

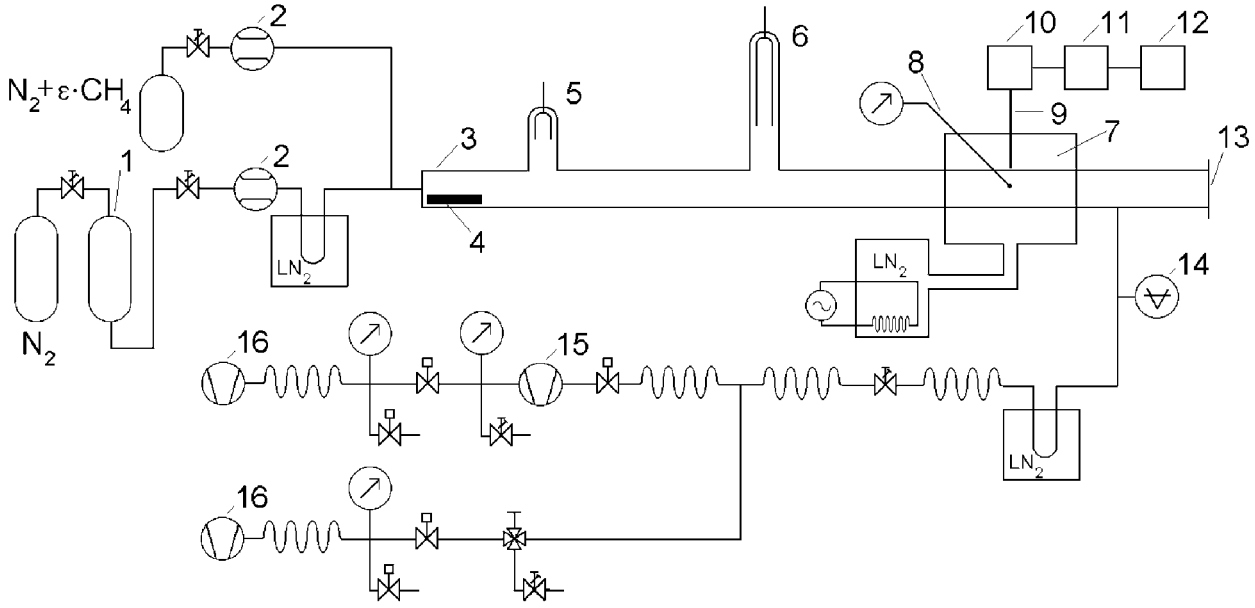

Fig. 1 Schematic drawing of the DC experimental device: 1 – Catalyzer, 2 – Mass flow controller, 3 – Pyrex discharge tube, 4 – Polymeric sample, 5 – Anode, 6 – Cathode, 7 – Cooled space, 8 – Thermocouple, 9 – Optical fiber, 10 – Monochromator, 11 – Optical multichannel analyzer, 12 – Personal computer, 13 – Input of samples, 14 – Pirani gauge, 15 – Diffusion pump, 16 – Rotary oil pump

All experiments in this study were done in the flowing regime. Total gas pressure is the other basic parameter of the experimental work. If the gas pressure is too low the collisions of heavy particles with walls of the post-discharge reactor play the dominant role. Under these conditions the heavy particle collisions in the gas phase could not be observed, or it was too difficult to separate these two types of processes (wall and volume processes). On the other hand at high pressures (near to the atmospheric pressure), the heavy particle collisions are very frequent and it is very difficult to separate various reaction channels. The role of three and more body processes significantly complicates the interpretation of the results, too. Due to these facts the gas pressures in the range of 100 – 2000 Pa are usually used for the kinetic studies during post-discharges.

The reactor dimensions also have significant influence on the observations, as it was mentioned before. The discharge cylindrical tube is used as a standard though sometimes other configurations can be used. The significant parameter of the afterglow tube is its diameter. The role of the wall processes increases with the increasing surface:volume ratio. Due to these facts the large diameter tubes are optimal. The wall processes are more significant with the decreasing the gas pressure, so the reactor diameter must be increased with the decreasing pressure. The inner diameter of 16 mm was used as sufficient for the experiments in this study. The wall processes, and their role in the kinetics, of course depend on the wall material. Usually, the Pyrex glass is used as a reactor material due to its relatively easy manufacturing. The nitrogen afterglow in this tube is very well visible up to the time of 1s and the optical emission spectroscopy can be applied very easily. Unfortunately, Pyrex has a considerable disadvantage – it absorbs the light under 300 nm. Another disadvantage is the higher efficiency of the wall reactions. The best material for the post-discharge reactor is Quartz. It has no limits for the use of optical emission spectroscopy and the efficiency of the wall processes is very low. The disadvantage of this material is in its very complicated manufacturing. In the presented study both materials were used.

The connection of the post-discharge tube to the active discharge can be axial or broken. The influence of the light coming directly from the active discharge can complicate the spectroscopic observations in the first of these configurations. On the other hand, this configuration allows measuring in the post-discharge from its beginning without time interruption. The use of black horn or

other non-axial connections of post-discharge region eliminate the active discharge influence but it is impossible to observe the earliest period of the afterglow. This second configuration was used in microwave set-up.

The last experimental parameter is type of an active discharge. In the presented studies two different discharge types were used; the DC and microwave. The microwave discharge is the electrodeless type of discharge where the electromagnetic energy (frequency 2450 MHz) is transferred into the plasma in special resonance cavity. The dissociation ratio in this type of discharge is higher and neutral gas temperature is lower than in the other case. The disadvantage is in the necessity to tune the microwave resonator to obtain the maximal energetic efficiency of the system. This problem is not significant in the DC discharge case. The electrodes (cathode and anode) are usually placed in the side arms of the main tube and the gas flows through the active discharge with less direct interaction with the electrodes. Due to the ion bombardment of the cathode some metal trace impurities are emitted into the gas flow, especially at higher discharge powers, and thus the purity of the studied gas is lower than in the microwave discharges. The dissociation ratio is lower and neutral gas temperature is higher than in the case when the other plasma source is used.

Table 1: Comparison of the experimental set-ups and experimental conditions

	MW Brno	**DC Orsay**	**DC Prague**	**DC Brno**
Plasma source	Microwave	DC	DC	DC
Electrodes	Electrodeless	Tantalum	Tantalum	Molybdenum
Afterglow tube	Quartz	Pyrex	Pyrex	Quartz
Cooling	Special arc tube	None	Liquid nitrogen vapor	Liquid nitrogen vapor
Afterglow wall temperature	77 and 300 K	300 K	77 – 300 K	77 – 300 K
Afterglow observation time	35 ms	0 – 50 ms	0 – 60 ms	0 – 60 ms
Total gas pressure	250 – 2000 Pa	665 Pa	665 and 2000 Pa	665 and 2000 Pa
Additional gas	None	None	Ar	None
Impurities	CH_4	CH_4	CH_4	CH_4 and halogenated hydrocarbons
Plastic materials	Not defined	None	Yes	Yes
Spectral range	200 – 610 nm	300 – 600 nm	300 – 800 nm	200 – 800 nm
Observed spectral systems	$N_2\ (B\ ^3\Pi_g) \rightarrow N_2\ (A\ ^3\Sigma_u^+)$ $N_2\ (C\ ^3\Pi_u) \rightarrow N_2\ (B\ ^3\Pi_g)$ $N_2^+\ (B\ ^2\Sigma_u^+) \rightarrow N_2^+\ (X\ ^2\Sigma_g^+)$ $CN\ (B\ ^2\Sigma^+) \rightarrow CN\ (X\ ^2\Sigma^+)$	$N_2\ (B\ ^3\Pi_g) \rightarrow N_2\ (A\ ^3\Sigma_u^+)$ $N_2\ (C\ ^3\Pi_u) \rightarrow N_2\ (B\ ^3\Pi_g)$ $N_2^+\ (B\ ^2\Sigma_u^+) \rightarrow N_2^+\ (X\ ^2\Sigma_g^+)$ $CN\ (B\ ^2\Sigma^+) \rightarrow CN\ (X\ ^2\Sigma^+)$	$N_2\ (B\ ^3\Pi_g) \rightarrow N_2\ (A\ ^3\Sigma_u^+)$ $N_2\ (C\ ^3\Pi_u) \rightarrow N_2\ (B\ ^3\Pi_g)$ $N_2^+\ (B\ ^2\Sigma_u^+) \rightarrow N_2^+\ (X\ ^2\Sigma_g^+)$ $CN\ (B\ ^2\Sigma^+) \rightarrow CN\ (X\ ^2\Sigma^+)$ $CN\ (A\ ^2\Pi) \rightarrow CN\ (X\ ^2\Sigma^+)$	$N_2\ (B\ ^3\Pi_g) \rightarrow N_2\ (A\ ^3\Sigma_u^+)$ $N_2\ (C\ ^3\Pi_u) \rightarrow N_2\ (B\ ^3\Pi_g)$ $N_2^+\ (B\ ^2\Sigma_u^+) \rightarrow N_2^+\ (X\ ^2\Sigma_g^+)$ $CN\ (B\ ^2\Sigma^+) \rightarrow CN\ (X\ ^2\Sigma^+)$ $CN\ (A\ ^2\Pi) \rightarrow CN\ (X\ ^2\Sigma^+)$

The technique of measurement at temperatures below the ambient is a separate problem. The experiments showed that cooling of the post-discharge region significantly decreases the time of the visible light emission. Due to this fact the cooling can be applied around the observation point only, from experience about ± 5 milliseconds. A computer simulations of the spectra show that in the center of this relatively small cooled volume the neutral gas temperature decreases down to 100 K, so the cooling is efficient enough. The practical realization of the cooling can be done by two systems. The post-discharge tube can be formed into the arc with the side observation input and immersed in liquid nitrogen (see Fig. 2). This configuration was used in the microwave experiments only. The advantage is good immersion without the possibility to change the temperature. The problem is also in the fixed

position of the observation point in the post-discharge time when the plasma source could not be movable.

The other practical cooling system uses the liquid nitrogen vapour let into the cooling box. The temperature can be continually changed and controlled and the box can be moved along the post-discharge tube. This system can be applied independently of the plasma source.

The exact experimental configurations used during the studies are presented in publications in appendices. The following table provides a short comparative overview of the experimental set-ups. This table shows the gases used during the experiments and the other necessary parameters.

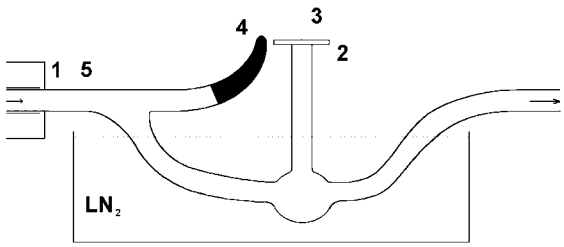

Fig. 2 Detail of the observation tube: 1 – Microwave resonator, 2 – Quartz window, 3 – Optical axis of the monochromator, 4 – Wood's horn covered by a black cloth, 5 – Active discharge

4 PURE NITROGEN POST-DISCHARGE

The post-discharge in pure nitrogen takes relatively long time until the relaxation of atomic and various metastable molecular states leads to the common thermal equilibrium. The relaxation constitutes various processes, that will be described in a separate section, and it is accompanied by the light radiation. The visible light can be recorded up to one second after switching off the active discharge, so in the flowing regime the radiation can be seen many meters from active discharge.

4.1 NITROGEN PINK AFTERGLOW

The earlier part of the pure nitrogen afterglow is described in Fig. 3. The strong light emission at about 7 – 14 ms after the end of an active discharge is known as a "pink afterglow" and it can be observed in nitrogen only. It is manifested by a strong increase of the pink light emission at the decay times of about 8 ms in pure nitrogen and of about 28 ms in nitrogen–argon mixture while the yellow–orange color is characteristic of the other parts of nitrogen afterglow. The nitrogen pink afterglow can be characterized as a secondary discharge because the electron concentration strongly increases due to the stepwise ionization [58, 59, 46] (see below in the section on kinetic processes) and thus the conditions are similar to those in the active discharge.

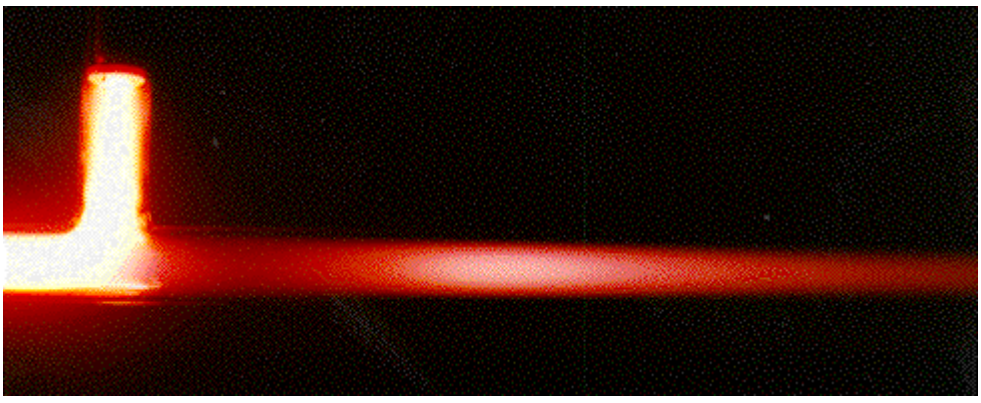

Fig. 3 Post-discharge in pure nitrogen

The pink afterglow was studied by electron paramagnetic resonance and microwave cavity spectroscopies [22] that allow direct measurement of the free electron concentration during the afterglow and also of some other paramagnetic species (for example nitrogen atoms) can be observed.

The free electron concentration strongly increases at the space of the pink afterglow. Also the concentration of the atomic species increases in this post-discharge region.

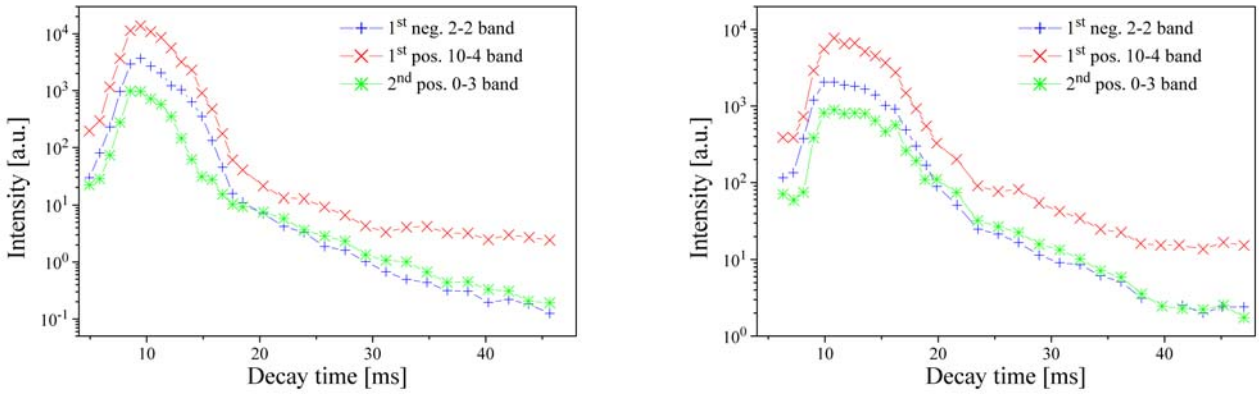

Fig. 4 Profile of the band head intensities of selected bands during the afterglow at the wall temperature of 300 K (left) and at 77 K (right)

Similar profiles during the post-discharge are also observed in the light radiation. Three nitrogen spectral systems mentioned above were studied during the pure nitrogen post-discharge. The profiles of selected bands of these systems are shown in Fig. 4 at two different wall temperatures. All these profiles correspond well with the visual observation (see Fig. 3) at ambient wall temperature. The pink afterglow effect can be well seen at low wall temperature, too, but its maximal intensity is somewhat lower than at a higher temperature. On the other hand, the pink afterglow maximum is not strictly located and is dispersed over a few milliseconds. Fig. 4 shows also the small enhancement of the light emission at about 25 ms, and at 28 ms, respectively. A similar effect was observed also in one other laboratory [11] but it is not too strong and no other data are available.

The later afterglow produces a significantly stronger light emission at a lower temperature. It can also be seen that the 1st negative emission decreases faster than the emission of the second positive system. The decrease of the first positive system is the slowest one but it is also enhanced by the nitrogen atomic recombination which will be discussed later.

4.2 VIBRATIONAL DISTRIBUTIONS DURING THE AFTERGLOW

The light emission of various nitrogen bands could not give sufficient information for more detailed studies of the kinetic processes running during the post-discharge. More effective are vibrational population studies of the upper states of the observed spectral transitions. The relative vibrational populations were calculated from the measured spectral intensities of the P_1 band heads using the wavelengths and transition probabilities given in [13]. The correction on the spectral sensitivity of the used spectrometer was of course included, too. The temperature of decaying plasma at the measuring point is also a significant parameter. This is demonstrated in Fig. 5 where at different conditions there are also present spectra of the higher nitrogen first positive system which are not usually observed.

The relative vibrational populations were calculated from the following band head intensities:

- for the N_2 ($B\ ^3\Pi_g$) state more than 40 vibrational bands, dominantly from the Δv = + 2, + 4 and + 5 sequences, in the spectral range of 505 – 585 and 705 – 780 nm
- for the N_2 ($C\ ^3\Pi_u$) state from the Δv = –2, –3 and –4 sequences (bands 2–4, 1–3, 0–2, 2–5, 1–4, 0–3, 4–8, 3–7 and 2–6)
- for the N_2^+ ($B\ ^2\Sigma_u^+$) state from the Δv = 0 and –1 sequences (2–2, 1–1, 0–0, 6–7, ... 0–1 bands).

When the band head was overlapped by another band, no population was calculated. When more transitions from the same vibrational level were observed the final population on that level was calculated as the average value of the populations calculated from the transitions.

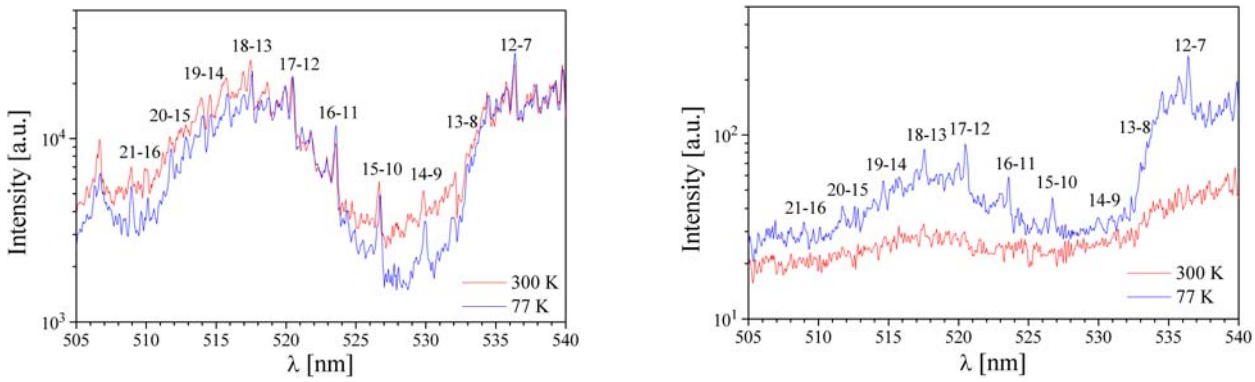

Fig. 5 A spectra of nitrogen first positive system (transitions originating at higher levels) in the pink afterglow (9 ms – left, 35 ms – right) at different wall temperatures

The vibrational distributions of the studied states are given in Figs. 6–8, for each state at two different wall temperatures. All of them clearly demonstrate the afterglow excitation enhancement during the pink afterglow with the maximum at the decay time of about 9 ms. The profiles of the vibrational distributions are shown only at six selected decay times chosen equidistantly.

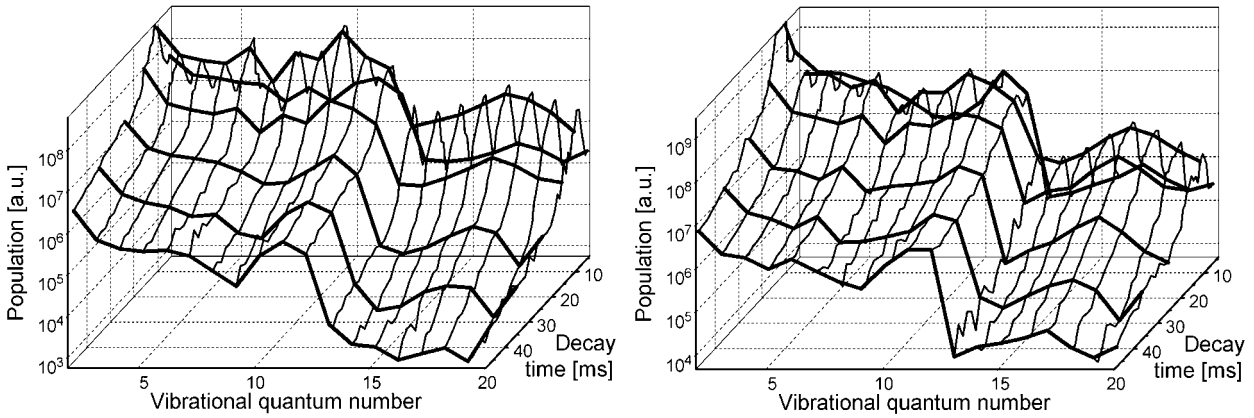

Fig. 6 Dependencies of the N_2 ($B\ ^3\Pi_g$) relative vibrational populations during the afterglow at the wall temperature of 300 K (left) and at 77 K (right)

The vibrational populations of the N_2 ($B\ ^3\Pi_g$) state are shown in Fig. 6. It can be clearly seen that at lower vibrational levels (up to $v = 7$) the distribution is nearly of Boltzmann type. Populations at the levels 10 – 12 are about two orders higher then extrapolation of Boltzmann distribution and this enhancement increases with the decay time. This effect is caused by the recombination of the ground state nitrogen atoms. The enhancement of population on $v = 12$ related to population on $v = 11$ at lower temperatures especially in later afterglow times was explained in the theory of nitrogen atom recombination given by *Partridge* [48] and will be discussed later. The populations on levels 8 and 9 are more complicated. In the later afterglow they show the Boltzmann distribution but in the pink afterglow the populations are increased. This enhancement can be the result of faster vibrational relaxation of the N_2 ($A'\ ^5\Sigma_g^+$) state, which is an intermediate state in the recombination, at higher temperatures.

The populations on levels lying just above the dissociation limit ($v = 13 – 15$) are relatively small, even in the pink afterglow where they could be directly populated also by electrons. Due to this fact the population minimum at these levels is not so deep as in the later afterglow. The higher lying levels ($v = 16 – 21$) are probably populated by any energy pooling reactions of the lower lying states. This explanation is based on an approximately identical slope in dependence of population on the decay time as it is for the lowest levels which are populated by this mechanism [53, 54, 55]. A detailed discussion of the possible kinetic processes populating these levels will be given in the section dedicated to the description of these processes. At the higher wall temperatures, the maximum of population among these levels can be seen at the levels $v = 17$ and 18, but at lower temperatures the

population on the level $v = 17$ is dominant, so the corresponding excitation reaction has a resonance character.

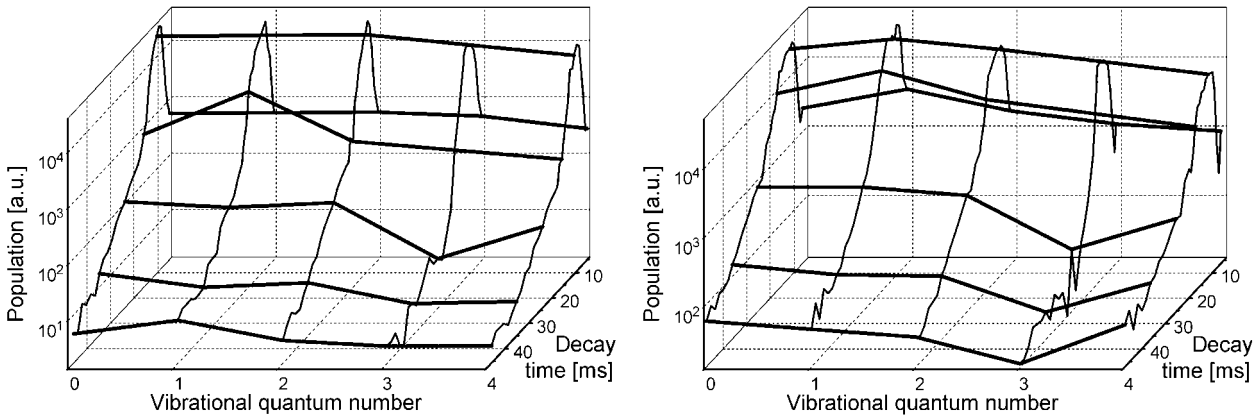

Fig. 7 Dependencies of the $N_2(C\ ^3\Pi_u)$ relative vibrational populations during the afterglow at the wall temperature of 300 K (left) and at 77 K (right)

The vibrational distributions of the $N_2(C\ ^3\Pi_u)$ state are shown in Fig. 7. The populations do not differ on the three lowest levels ($v = 0 – 3$). The population on the level $v = 3$ is not too accurate because the bands corresponding to the transitions from this level are strongly overlapped by the rotational structure of the nitrogen first negative bands. These bands cannot be resolved in the pink afterglow spectrum, so the experimental points are not present in the graphs. The population on the level $v = 4$ in the pink afterglow is lower than the populations on the lower levels due to the possible predissociation into the $N(^4S_0)$ and $N(^2D_0)$ atoms. On the other hand, the recombination of these atoms is the precursor for enhancement of the population on this level during the later afterglow, especially at a low temperature.

Fig. 8 presents the vibrational populations of the $N_2^+(B\ ^2\Sigma_u^+)$ state. The populations of all vibrational levels strongly depend on the decay time in comparison with the neutral nitrogen states. Strong enhancement in the pink afterglow results in the stepwise ionization and the consequential vibrational energy transfer between the ground state of the vibrational excited neutral nitrogen and the ground state of the nitrogen molecular ion. The strong population quenching is realized by an electron–ion recombination. The populations during the earlier afterglow are close to the Boltzmann populations at the lower vibrational levels, the higher level populations are almost independent on any levels. The inversion in higher level populations can be observed during the later afterglow.

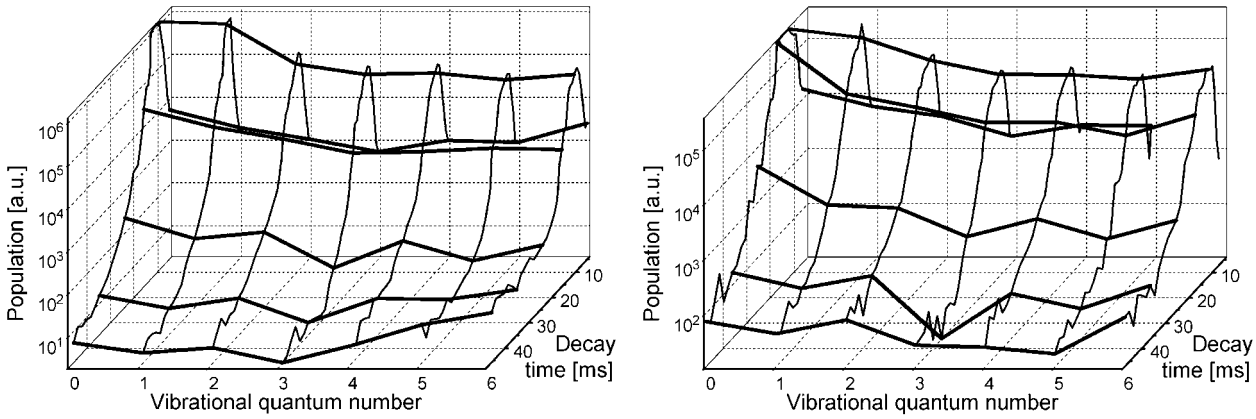

Fig. 8 Dependencies of the $N_2^+(B\ ^2\Sigma_u^+)$ relative vibrational populations during the afterglow at the wall temperature of 300 K (left) and at 77 K (right)

4.3 COMPARISON OF AFTERGLOWS WITH AN ACTIVE DISCHARGE

This paragraph gives a short comparison of the N_2 ($B\ ^3\Pi_g$) relative vibrational distributions in an active microwave discharge and in afterglows at the wall temperatures of 300 K and 77 K. The results are presented in Fig. 9. Absolute values of the measured vibrational band intensities also depend on the experimental conditions. Intensities observed in the active discharge are much higher than in the afterglow, but intensities in the afterglow are comparable each to others. Due to this fact the populations were adjusted to the N_2 ($B\ ^3\Pi_g$, $v = 12$) vibrational level. For the description it is useful to study the distribution changes on levels under the predissociation limit ($v \leq 12$) and on levels above this limit separately. The population on the level $v = 13$ could not be computed due to a very low measured intensity of the corresponding bands.

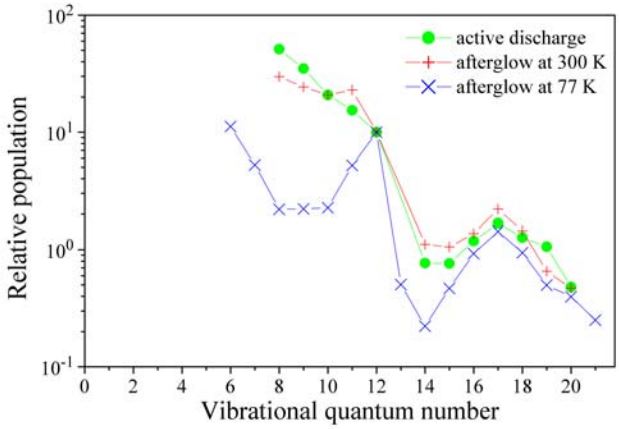

Fig. 9 Vibrational distribution of N_2 ($B\ ^3\Pi_g$) state in the active microwave discharge and in its afterglows at the 300 K and 77 K wall temperatures (all populations are normalized to level $v = 12$

In an active discharge, the vibrational distributions at lower levels have a usual Boltzmann character. In the afterglow at room wall temperature the character of the distribution is nearly the same, only the population on the level $v = 11$ is about 50 % higher than the Boltzmann estimated value. The populations at the higher vibrational levels are not so high as in the active discharge, either. In the afterglow at the lower wall temperature the distribution is completely different. At the lower vibrational levels (under $v = 10$) the Boltzmann character of the distribution is maintained, but on the levels $v = 11$ and 12 an overpopulation can be observed. This is the result of the three body recombination process, as it will be mentioned later.

The vibrational distribution on higher N_2 ($B\ ^3\Pi_g$) levels does not show such strong differences as those on the lower levels. In all three studied cases, the maximum population on the $v = 17$ level is observed. This maximum becomes stronger in the afterglow, especially at a low temperature. The redistribution to lower levels in the afterglow is observed, too.

The experimental results have been compared with the other studies, too. The main problem was that each author used different conditions. The details of these studies can be found in [33].

5 AFTERGLOW IN THE NITROGEN–METHANE GAS MIXTURES

There is a huge number of studies inquire into the discharges and post-discharges in nitrogen–methane gas mixture for different applications. Usually the methane concentrations higher then 1 % are used, for example in deposition of the C_xN_y layers [37, 78] or during the study of extraterrestrial life possibility [66]. The studies oriented to the problem of the influence of methane traces on the pure nitrogen afterglow are relatively rare.

The flowing nitrogen post-discharge has appeared during last years in the new field of extremely sensitive spectral emission methods and techniques, designed especially for the detection of impurities containing carbon and oxygen. Besides the emission of three nitrogen spectral systems observed in the pure nitrogen, the emission of the CN violet (CN ($B\ ^2\Sigma^+$) → CN ($X\ ^2\Sigma^+$)) and red (CN ($A\ ^2\Pi$) → CN ($X\ ^2\Sigma^+$)) spectral systems has been widely observed as in the reactions of active nitrogen with hydrocarbons and partially or fully halogenated hydrocarbons [69, 14, 73, 18, 24], usually at relatively high hydrocarbon concentrations in range percents. The upper electronic states of these two spectral systems (CN ($B\ ^2\Sigma^+$) and CN ($A\ ^2\Pi$)) are formed preferentially in selected vibrational states. There are

also many state specific collisional energy transfer reaction with vibrationally excited nitrogen ground state [23, 30]. The effects coupled with these kinetic reactions have been discussed in many works [34, 26] but only as a "parasitic effect".

The extensive research may lead to many applications in the field of environmental analysis (e.g. monitoring of trace hydrocarbon impurities during plasmachemical nitridation, analyzing the air, water and food quality, etc.) and the basic research, too. This section gives a review of the observed phenomena in the pure nitrogen containing the methane traces in wide range from 0.01 ppm up to about 400 ppm. The experimental set-up allow to study the dependencies of vibrational distribution of the N_2 ($B\ ^3\Pi_g$) and CN ($A\ ^2\Pi$) states, the second one in the DC post-discharge only. The other possible states (N_2^+ ($B\ ^2\Sigma_u^+$), N_2 ($C\ ^3\Pi_u$) and CN ($B\ ^2\Sigma^+$) are presented only by the dependencies of the band intensities of some of the spectral bands originated at these states because the spectral bands are usually overlapped and thus it is impossible to obtain the vibrational populations at more levels in wide range of methane concentrations.

5.1 QUENCHING OF THE NITROGEN PINK AFTERGLOW

The nitrogen pink afterglow in pure nitrogen was shown in the previous paragraph as a well known effect manifested by the strong increase of the pink light emission at the decay times of about 8 ms. The step-wise ionization process strongly depends on the presence of impurities in the pure nitrogen. The methane concentrations of about 10 ppm can fully destroy the effect of the pink afterglow [31].

The effect of the pink afterglow quenching was studied using the DC flowing post-discharge devices at the total gas pressure of 1000 Pa without cooling the discharge tube walls. The total gas flow during these experiments was fixed at 600 ml min^{-1} with discharge power of 170 W. These conditions allow the direct visual observations as well as the spectroscopic measurements and the influence of the CN spectra has been much smaller then at decreased temperature.

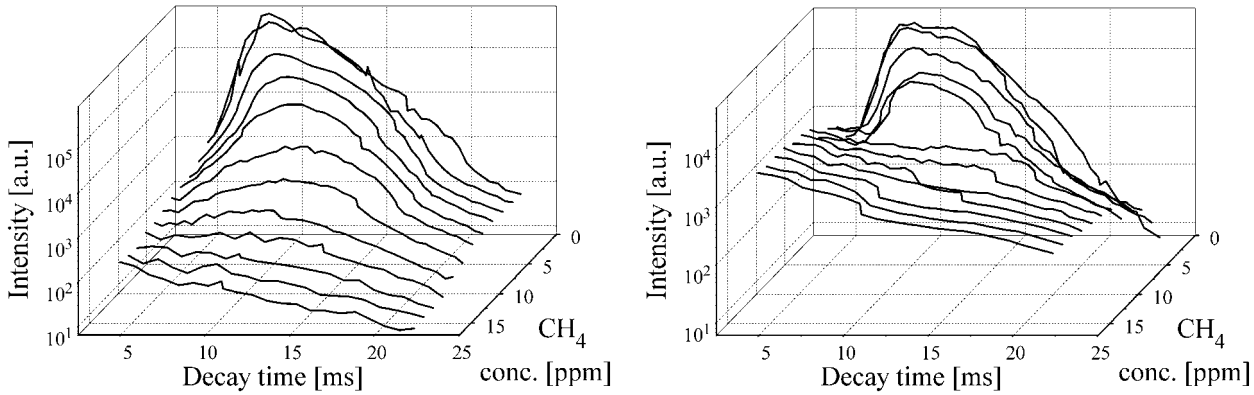

Fig. 10 1st neg. 0–0 band head intensity profiles (left) and 1st neg. 1–1 band head intensity profiles overlapped by CN violet 0–0 band (right) in relation to the methane concentration

The influence of methane presence on the pink afterglow has been observed through the emission of the nitrogen 1st neg. and CN violet spectral systems, the nitrogen 1st and 2nd pos. systems have been used as a reference only. The other spectral systems have been observed only in the other experiments and they are presented in next subsections. Fig. 10 shows measured band head intensities of selected bands as a function of the methane concentration during the pink afterglow. The intensity profiles of the 1st neg. 0–0 and both nitrogen positive systems are similar and thus they are not presented here. Different situation is in the case of 1st neg. 1–1 band which is completely overlapped by the P branch of 0–0 CN violet spectral system. Thus at methane concentrations up to 7 ppm the effect of the pink afterglow can be resolved, at higher concentration the strong CN emission state can be dominant and its intensity is more or less independent of the methane concentration in the studied range.

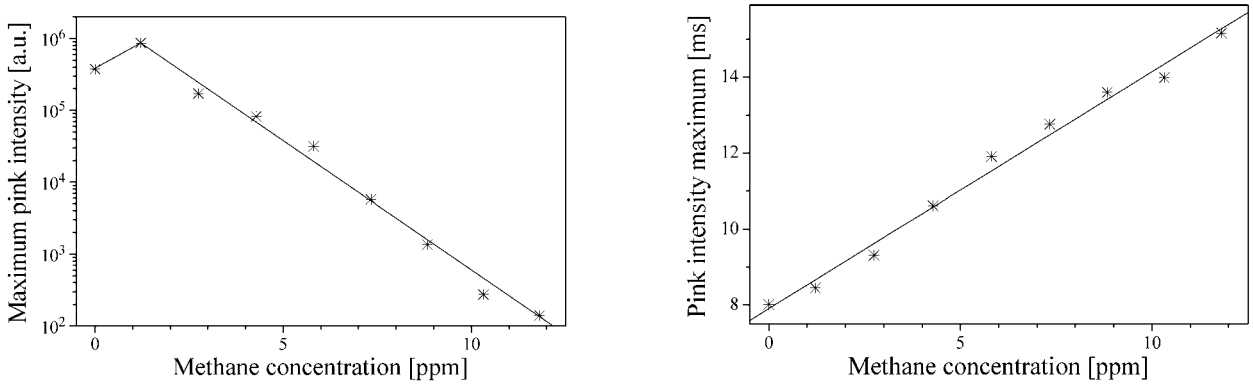

Fig. 11 Maximum intensity of the pink afterglow emission and its position as a function of methane concentration

Fig. 11 is more illustrative. It shows the dependence of the pink afterglow maximum intensity on the methane concentration. A small increase of the intensity can be seen at methane concentrations up to about 1 ppm and thereafter the maximum intensity is exponentially quenched by methane. At concentrations higher then 12 ppm the maximum of the pink afterglow can't be found, however, this effect still exists. Fig. 11 also demonstrates the shift of the pink afterglow intensity maximum to later decay times. This effect is directly proportional to the methane concentration. In pure nitrogen the pink afterglow intensity maximum can be seen at decay time of 8 ms and this result is in excellent agreement with previous studies [6]. The maximum pink intensity shifts up to 15.5 ms at the highest methane concentration of about 12 ppm when the effect can be measured.

5.2 VIBRATIONAL DISTRIBUTIONS OF N_2 ($B\ ^3\Pi_g$) STATE IN MICROWAVE AFTERGLOW

Dependencies of N_2 ($B\ ^3\Pi_g$) vibrational distribution on the very low methane concentration have been studied in the microwave afterglow only at low (77 K) wall temperature. The populations have been computed from the measured intensities of $\Delta v = +4$ and $+5$ sequences. In cases when the intensities from both sequences were available, the average population has been used. When two bands were overlapping (it is case of 19–15 with 10–5 bands), the populations have not been determined. For the 20–15 and 19–14 bands, the overlapping 8–2 and 7–1 bands, respectively, play an insignificant role due to the fact that their Einstein coefficients are more than three orders lower and thus the corresponding band intensities could be neglected.

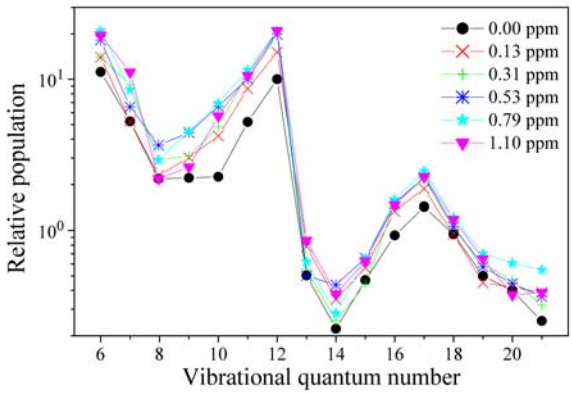

Fig. 12 Vibrational distribution of the N_2 ($B\ ^3\Pi_g$) state at different methane concentrations

The results are shown on Fig. 12. The population on the level 12 in pure nitrogen afterglow has been chosen as a reference value. From this figure it can be clearly seen that there are three maxims in vibrational population. The first one at low vibrational levels, the second one at level N_2 ($B\ ^3\Pi_g$, $v = 12$) and the third one at level N_2 ($B\ ^3\Pi_g$, $v = 17$). This clearly demonstrates different population mechanisms:

- In the first case, a common Boltzmann distribution, caused from the excitation by electrons in an active discharge, can be observed;
- In the second case, the three body recombination of nitrogen atoms is the main process;
- In the last case, the levels are populated by other processes.

All these processes will be described in details later. This paragraph gives only the description and short comments of the observed phenomena. The deep minimum at levels N_2 ($B\ ^3\Pi_g$, v = 13, 14) is the consequence of the predissociation.

From Fig. 12 it can also be seen that the vibrational populations change with a methane addition. Only the low methane concentrations in small concentration range have been used in the microwave post-discharge and also the position in the afterglow has been fixed. The data presented in this paragraph will be compared with more complex study of the methane influence on the nitrogen DC post-discharge given in the next paragraph.

5.3 VIBRATIONAL DISTRIBUTIONS OF THE N_2 ($B\ ^3\Pi_g$) STATE IN THE DC AFTERGLOW

The DC experimental set-up allows more thorough studies than the microwave one. Besides the temperature and methane concentration, the observation positions during the post-discharge were changed at this configuration. The methane concentration could be varied in a very wide range over more than four orders. Due to these facts, the experimental data are presented in more graphs.

The figures 13 – 15 present the vibrational distributions of the N_2 ($B\ ^3\Pi_g$) state at two wall temperatures at three different methane concentrations during the afterglow. The first post-discharge position (at 5 ms) is located in the middle between the active discharge and the maximum of the pink afterglow, the second one (at 11 ms) corresponds to the central position of the pink afterglow maximum (see Fig. 11). The third position (46 ms) corresponds to the Lewis-Rayleigh afterglow of nitrogen.

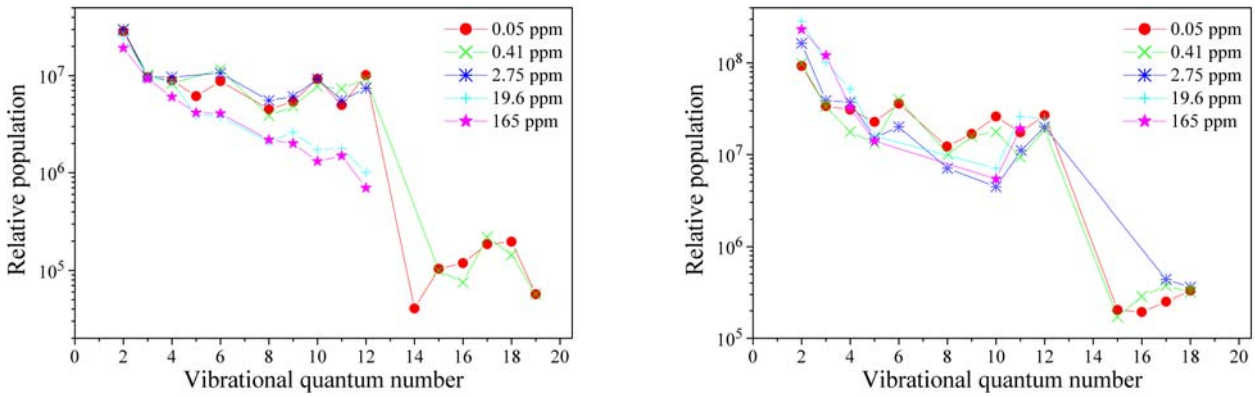

Fig. 13 Vibrational distributions of the N_2 ($B\ ^3\Pi_g$) state as a function of the methane concentration at the decay time of 5 ms at the wall temperature of 300 K (left) and at 77 K (right)

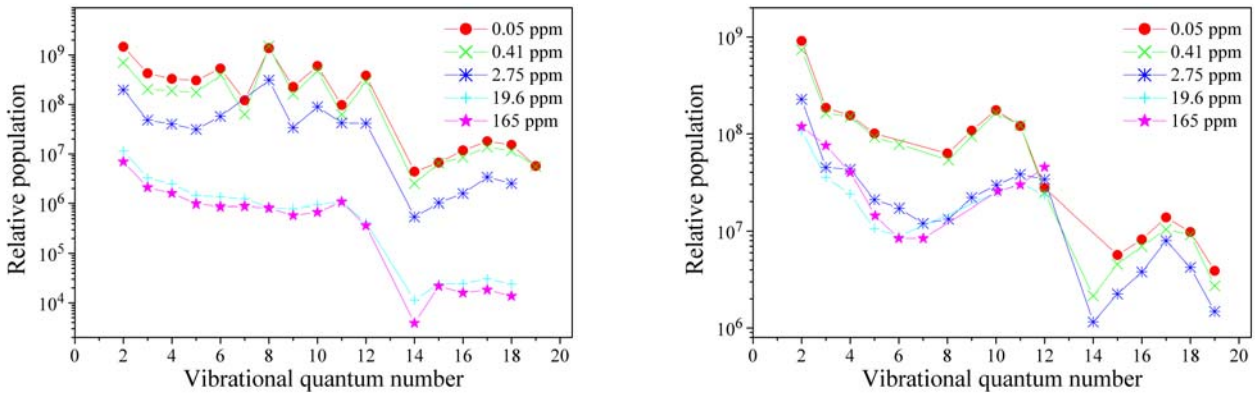

Fig. 14 Vibrational distributions of the N_2 ($B\ ^3\Pi_g$) state as a function of the methane concentration at the decay time of 11 ms at the wall temperature of 300 K (left) and at 77 K (right)

The vibrational distributions at the first positions in the discharge (5 ms) at an ambient wall temperature show a non-Boltzmann character at the lower methane concentrations because the levels

6 – 12 are at this time dominantly populated by the recombination of nitrogen atoms. At the higher methane concentrations the distribution is completely changed and it is more or less Boltzmann. This effect results probably from the decrease of the atomic nitrogen concentration because more nitrogen atoms recombine with the carbon atoms and thus create the CN radicals instead of the diatomic nitrogen molecules in the N_2 ($B\ ^3\Pi_g$) state. A similar effect can be observed also at the decreased wall temperature except for the levels 11 and 12 where the population is not significantly decreased by a methane addition. This will be probably due to the higher efficiency of atomic nitrogen recombination to these two levels at the lower temperature (see below).

The vibrational distributions measured in the pink afterglow at an ambient wall temperature (Fig. 14 left) shows the effect of the pink afterglow quenching at the methane concentrations higher than a few ppm. Profiles of the vibrational distributions are more or less independent of the methane concentration at all the levels lying below the predissociation limit (v = 12). The levels above this limit are at low methane concentrations populated especially at levels v =16 – 18, at higher methane presence no population preference can be observed. This phenomenon is probably connected with the changes in the vibrational distribution of the N_2 ($X\ ^1\Sigma_g^+$) state [32], as it will be discussed later. At the lower wall temperature, the effect of the pink afterglow quenching can be seen only at the decay time of 11 ms, later this effect could not be measured. The influence of the methane presence on the populations at the higher vibrational levels could not be determined due to the overlap of the corresponding nitrogen 1st pos. spectral band and the CN red spectral system.

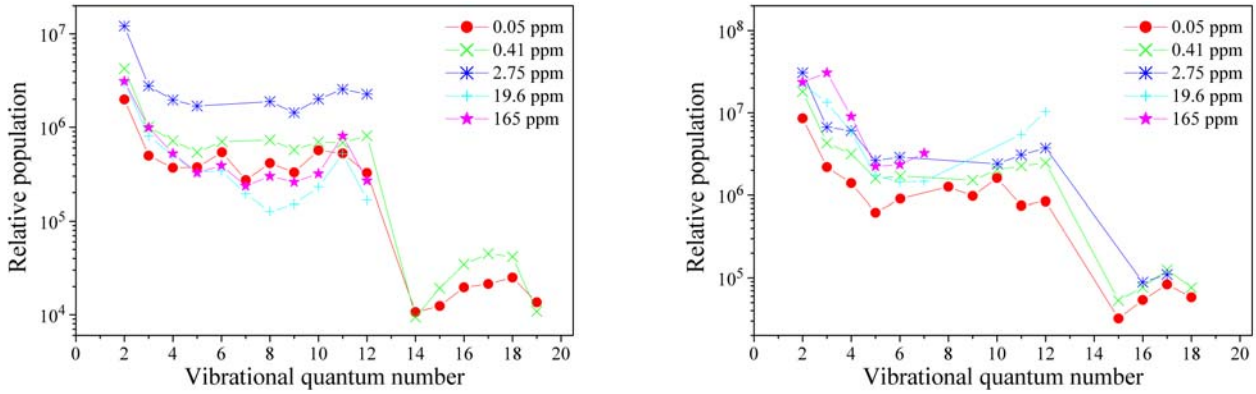

Fig. 15 Vibrational distributions of the N_2 ($B\ ^3\Pi_g$) state as a function of the methane concentration at the decay time of 46 ms at the wall temperature of 300 K (left) and at 77 K (right)

The increase of the populations at all vibrational levels can be seen at the latest observed decay time (46 ms) but at the ambient wall temperature this effect is not as strong as at a lower temperature. The profile of the vibrational distribution shows that at the higher methane concentrations the populations at the levels just below the predissociation limit increase especially at a lower wall temperature. This could be caused by an increase of the atomic nitrogen recombination.

The dependencies of vibrational distribution on methane concentration show the same three different groups of the vibrational levels as in pure nitrogen. For a more exact description of the population dependence on the methane concentration, four different vibrational levels were chosen; the level v = 2 that is dominantly populated by pooling reactions (see below), v = 11 and 12 populated preferentially by an atomic nitrogen recombination and level v = 17 as a representative of the higher vibrational levels. Fig. 16 – 19 present the populations at these levels as a function of the methane concentration at both wall temperatures. The decay times of 5, 11 and 35 ms were chosen to describe the situation in the early afterglow before the pink afterglow, in the pink afterglow and in the later Lewis-Rayleigh afterglow.

All selected levels show a strong quenching of the population at the methane concentration of a few ppm at the decay time of 11 ms. This corresponds to the quenching of the pink afterglow as it was described before. This effect is more than one order smaller at the lower wall temperature.

A specific situation can be observed at level $v = 12$ which did not show the pink afterglow effect at the low wall temperature. This could be explained by a possible predissociation of this state.

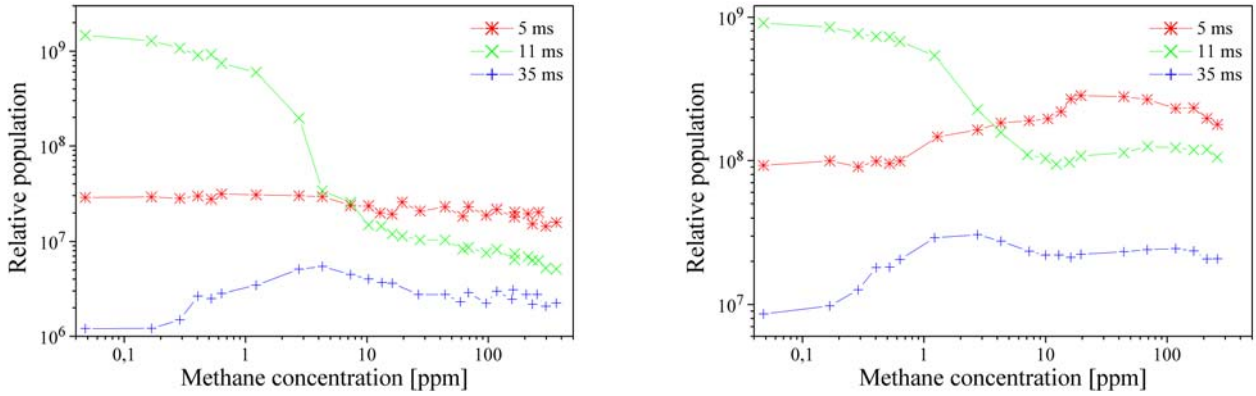

Fig. 16 The N_2 ($B\ ^3\Pi_g$, $v = 2$) population as a function of the methane concentration at different decay times at the wall temperature of 300 K (left) and at 77 K (right)

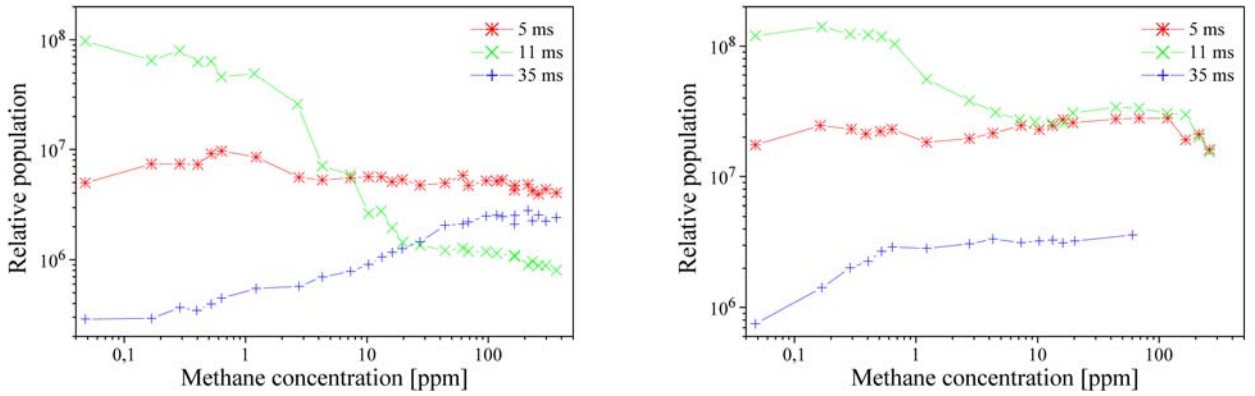

Fig. 17 The N_2 ($B\ ^3\Pi_g$, $v = 11$) population as a function of the methane concentration at different decay times at the wall temperature of 300 K (left) and at 77 K (right)

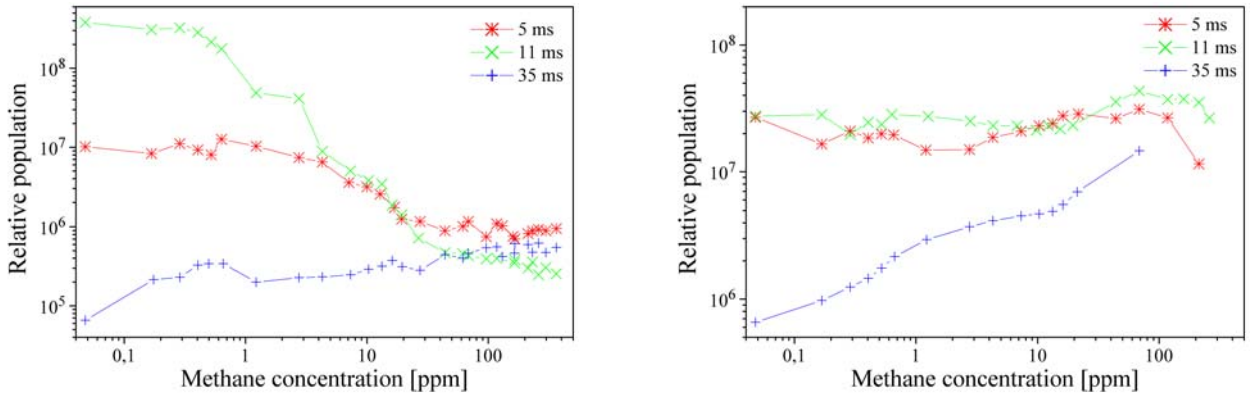

Fig. 18 The N_2 ($B\ ^3\Pi_g$, $v = 12$) population as a function of the methane concentration at different decay times at the wall temperature of 300 K (left) and at 77 K (right)

The afterglow before the pink afterglow did not show any significant dependence of the populations at the levels $v = 2$ and 11 at an ambient wall temperature, a slight increase (about three times, see Fig. 16 and 17) of the populations can be seen at a lower temperature. The population at the level $v = 12$ decreases about one order at an ambient temperature (Fig. 18), at the low wall temperature no dependence of the population on the methane concentration can be observed. The population at the level $v = 17$ shows a slight increase at the lower wall temperature, but the data are available for lower methane concentrations, only.

Finally, the increase of the populations at all the studied levels with the increasing methane concentration can be seen at both temperatures. The level $v = 2$ shows after an initial increase some

saturation of the population at the methane concentrations higher than a few ppm at both temperatures. The saturation could also be seen at the level $v = 11$ at a lower temperature, only. The population at the level $v = 12$ increases by about one order in the whole studied range of methane concentrations. The same situation could be observed also at the level 17 but in this case only a few data at the lower methane concentrations are available.

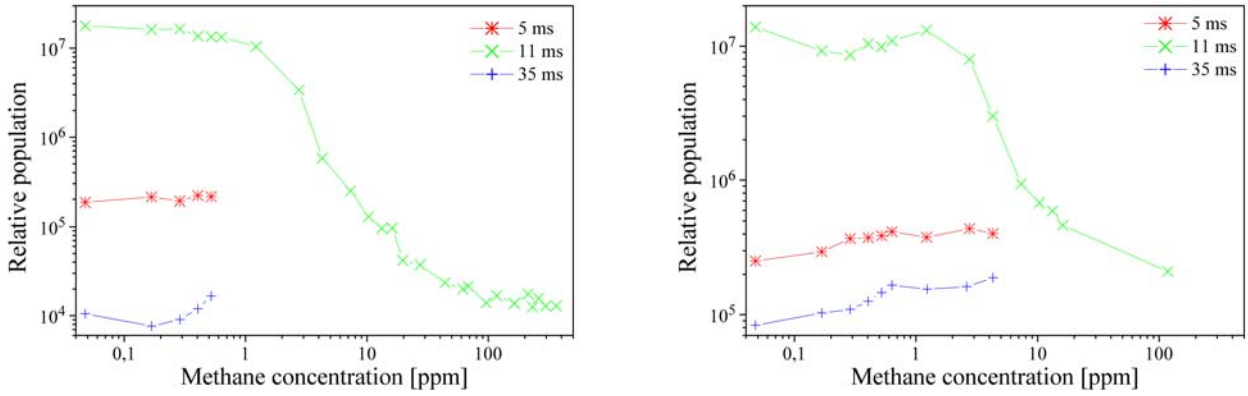

Fig. 19 The N_2 ($B\ ^3\Pi_g$, $v = 17$) population as a function of the methane concentration at different decay times at the wall temperature of 300 K (left) and at 77 K (right)

5.4 VIBRATIONAL DISTRIBUTIONS OF THE CN ($A\ ^2\Pi$) STATE IN THE DC AFTERGLOW

The vibrational distributions were obtained between the vibrational levels 4 and 9. The populations were calculated from the spectra of +3 and +6 sequences. The population at level 8 could not be obtained at all the experimental conditions due to the significant overlap of the CN red system 8–2 band, from which the population was calculated, by the rotational structure of the strong 1st pos. 12–7 band.

The experimental data are presented in Figures 20 – 22. The populations are presented only at higher methane concentrations because the CN red system (CN ($A\ ^2\Pi$) → CN ($X\ ^2\Sigma^+$)) bands are in the same spectral range as the intensive 1st pos. nitrogen system.

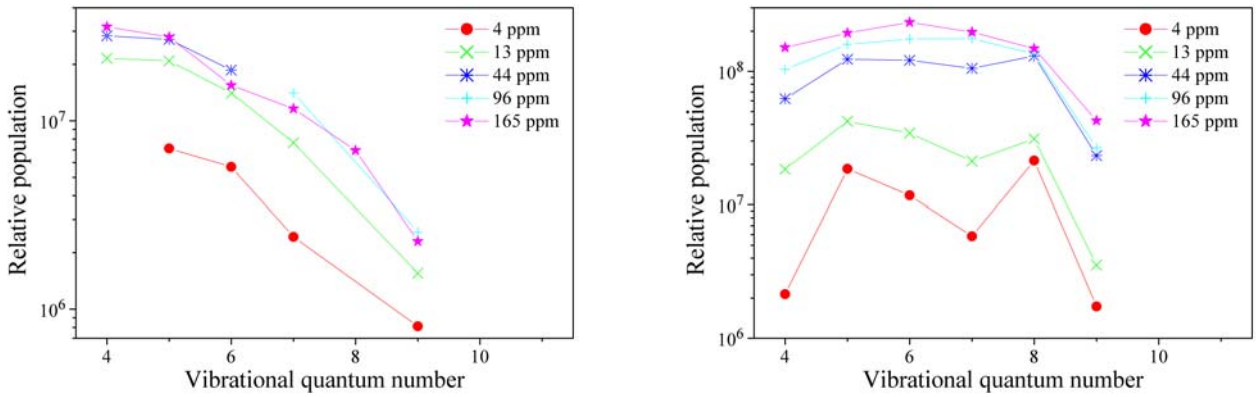

Fig. 20 Vibrational distributions of the CN ($A\ ^2\Pi$) state as a function of the methane concentration at the decay time of 5 ms at the wall temperature of 300 K (left) and at 77 K (right)

The distributions obtained at the ambient wall temperature in the region between an active discharge and the pink afterglow show more or less a Boltzmann character except for three points at levels 4 and 5. These values are probably incorrect due to the overlap of the corresponding bands by nitrogen bands. This distribution character could confirm the idea of population mechanisms of these levels as it will be discussed below. The distributions are completely changed at the lower wall temperature. The populations strongly increase at all the observed levels. The distribution observed at 4 ppm of methane shows that the populations among the vibrational levels differ by up to one order.

No significant differences among the populations at levels 4 – 8 can be observed at the highest studied methane concentration, the population at level 9 is equal to about one third of the other populations.

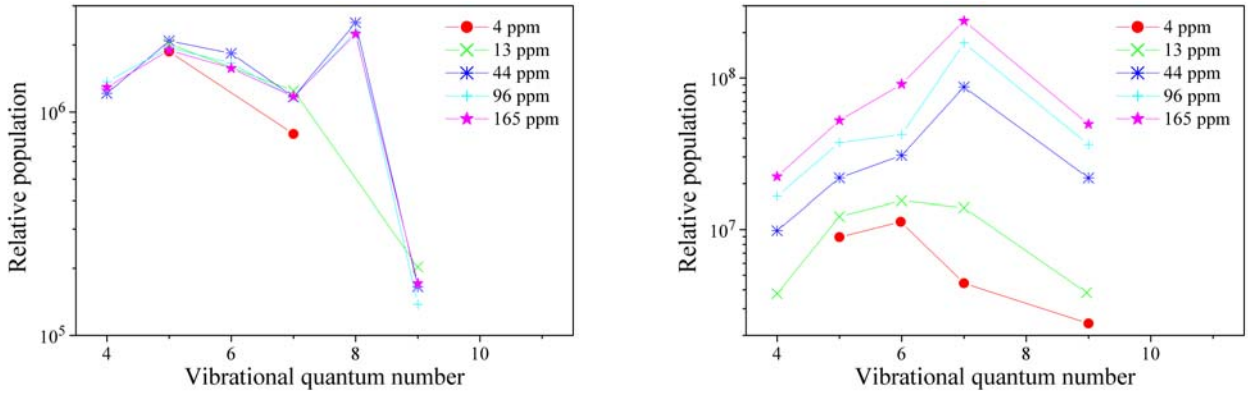

Fig. 21 Vibrational distributions of the CN (A $^2\Pi$) state as a function of the methane concentration at the decay time of 11 ms at the wall temperature of 300 K (left) and at 77 K (right)

The vibrational populations measured at the pink afterglow positions (the decay time of 11 ms, see Fig. 21) at the ambient wall temperature are more or less independent of the methane concentration and the vibrational distribution did not show any dependence, either. A different situation can be seen at the wall temperature of 77 K. The populations at all the levels are more than ten times higher than at the ambient wall temperature. The populations at all the observed levels increase with the increasing methane presence. The distribution among the levels 4 and 7 shows a strong inversion in the populations and this character is at the methane concentrations above 40 ppm nearly constant. The populations at levels 8 and 9 correspond more to a thermal distribution.

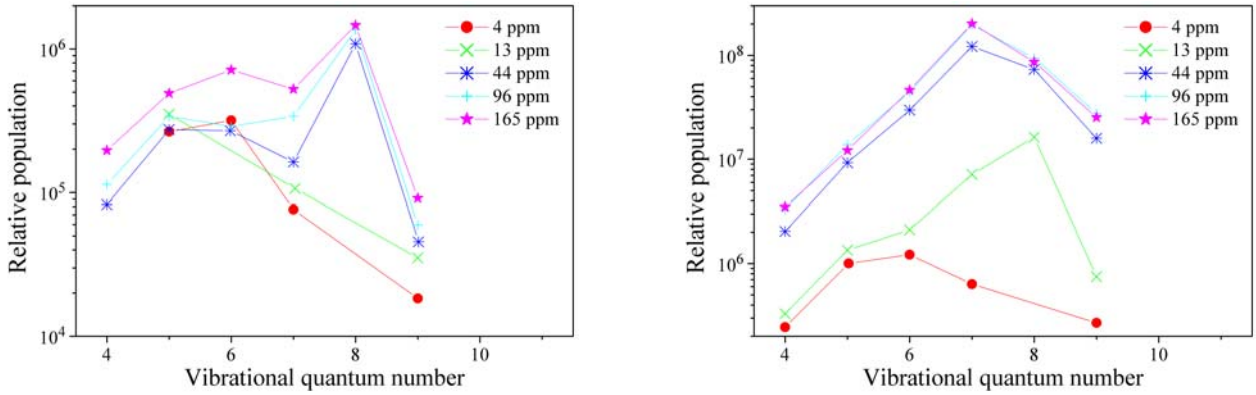

Fig. 22 Vibrational distributions of the CN (A $^2\Pi$) state as a function of the methane concentration at the decay time of 46 ms at the wall temperature of 300 K (left) and at 77 K (right)

Vibrational distributions measured in the later afterglow at an ambient wall temperature show a slow increase of the populations at all the levels with an increase of the methane concentration. The vibrational distribution during the post-discharge resembles more the distribution observed in the pink afterglow at low temperature, the population at level 8 is the highest one and it is nearly constant. The character of distribution at the decreased wall temperature is about the same as in the pink afterglow. It can be seen that the populations at the methane concentrations over 100 ppm are independent of the methane concentration.

The vibrational levels v = 5 and 9 were chosen to describe the vibrational population dependencies on the methane concentration more exactly. The experimental results are shown in Fig. 23 and 24 at the decay times of 5, 11, and 35 ms (the same as in the case of the N_2 (B $^3\Pi_g$) state). Figures 25a and 26a show clearly the independence of the vibrational population on methane concentration at the pink afterglow position and a slow increase of the population during the early and later afterglow. The dependencies observed at the low wall temperature show a strong increase of the populations during

the whole post-discharge, the saturation effect can be seen at the highest methane concentrations in the pink afterglow position and in the late afterglow it is possible to observe even a decrease of the population.

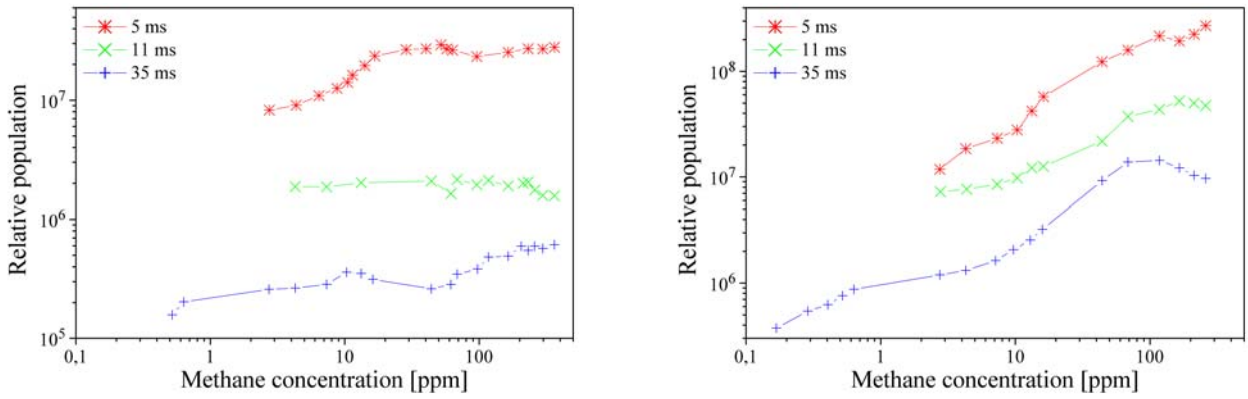

Fig. 23 The CN (A $^2\Pi$, $v = 5$) population as a function of the methane concentration at different decay times at the wall temperature of 300 K (left) and at 77 K (right)

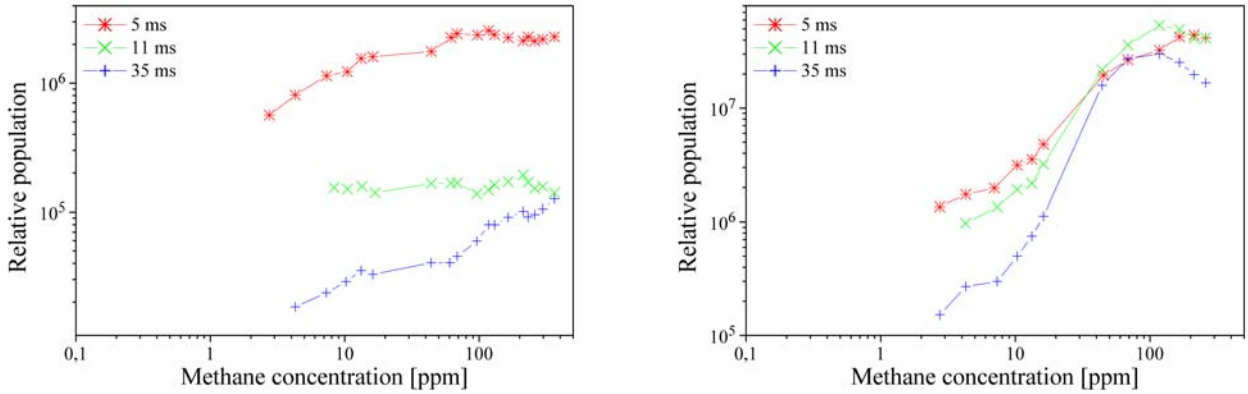

Fig. 24 The CN (A $^2\Pi$, $v = 9$) population as a function of the methane concentration at different decay times at the wall temperature of 300 K (left) and at 77 K (right)

5.5 THE RELATIONS AMONG THE NITROGEN 1ST NEG. AND 2ND POS. AND CN VIOLET BAND HEAD INTENSITIES AND METHANE CONCENTRATION

The last paragraph discusses the dependencies of vibrational distributions of N_2 (B $^3\Pi_g$) and CN (A $^2\Pi$) states during the post-discharge on the methane concentration. The dependencies of the other observed spectral bands, i.e. nitrogen 1st neg. and 2nd pos. and CN violet bands, will be presented now. These spectral systems have their bands relatively close to the others and thus they are often overlapped by other bands and spectral systems. Due to this fact it is very complicated to calculate the vibrational distributions of the corresponding upper states of these transitions. Another reason why the distribution could not be calculated is that many nitrogen bands are missing (or their intensities are too close to the noise level) at higher methane concentrations and, on the other hand, many CN bands cannot be observed at lower concentrations. Thus the 1st neg. 0–0, 2nd pos. 1–3 band head intensities are presented here by the methane concentration at two different wall temperatures and at six different decay times. These bands are the best-resolved bands of these systems and they could be considered highly representative as far as a study of their qualities is concerned. The CN violet system can be represented by three different bands, whose upper levels are populated by different mechanisms; the CN 0–0 band, which is strongly overlapped by the 1st neg. 1–1 band, represents the lowest CN (B $^2\Sigma^+$) levels that are excited by collisions with vibrationally excited nitrogen ground state molecules (see below), the band 7–7 originates from the recombination of nitrogen and carbon ground state atoms and finally the 12–12 band represents the transitions from levels lying over the CN (B $^2\Sigma^+$)

predissociation limit (at the level $v = 7$). Due to the fact that the transitions originated at these higher vibrational levels are not commonly observed, Fig. 25 shows an example of the corresponding spectrum.

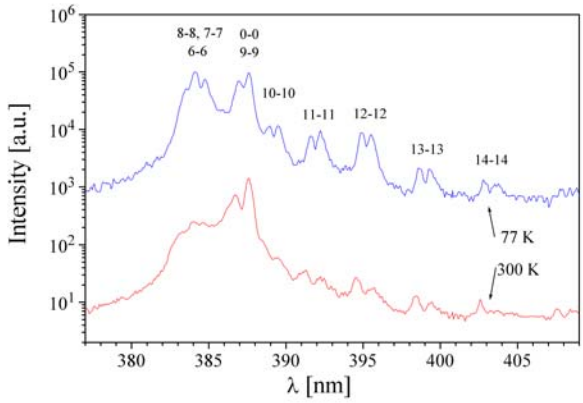

Fig. 25 CN violet spectrum for the decay time 46 ms at the methane concentration of 655 ppm

Fig. 26 presents the results obtained for 1st neg. 0–0 band. The dependencies are similar for both of the wall temperatures. The intensities are higher in the pink afterglow, before the pink the intensity is about the same, in the later afterglow the intensity is higher at the lower temperature. The quenching of the pink afterglow can be seen clearly at the decay times of 11 and 16 ms and it is stronger at an ambient temperature. An increase of the intensity can be seen at the lowest methane concentration at the decay time of 5 ms, at the concentration higher than 1 ppm the quenching is observed but both of these dependencies are slight only.

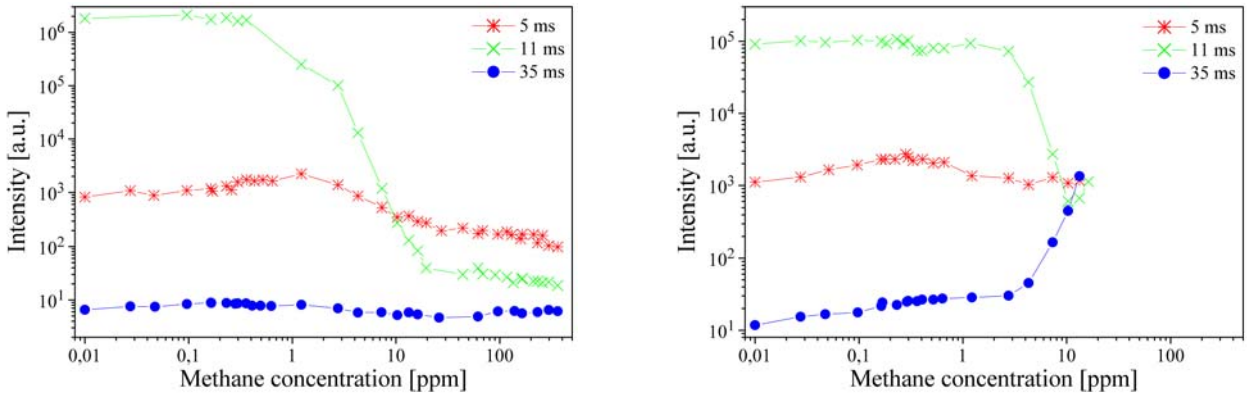

Fig. 26 The nitrogen 1st neg. 0–0 band intensity as a function of the methane concentration at different decay times at the wall temperature of 300 K (left) and at 77 K (right)

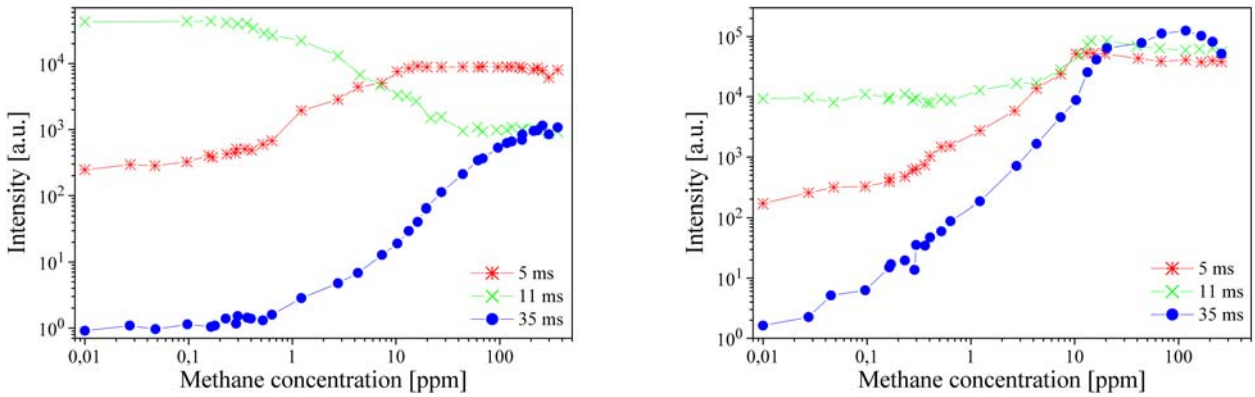

Fig. 27 The nitrogen 1st neg. 1–1 band intensity overlapped by CN violet 0–0 band as a function of methane concentration at different decay times at temperatures of 300 K (left) and 77 K (right)

A slight increase of intensity can be seen at the lower temperature at the decay time of 35 ms which could be coupled with the edge of the "pink afterglow". No evidence of it is present in the latest post-discharge position. The significant increase of the intensities at later afterglow positions at methane concentrations above 1 ppm at 77 K (resp. above 10 ppm at 300 K) results from the overlap of the 1st neg. 0–0 band by the CN violet 11–11 band (see the spectrum in Fig. 25) which could not be deconvoluted from the spectrum.

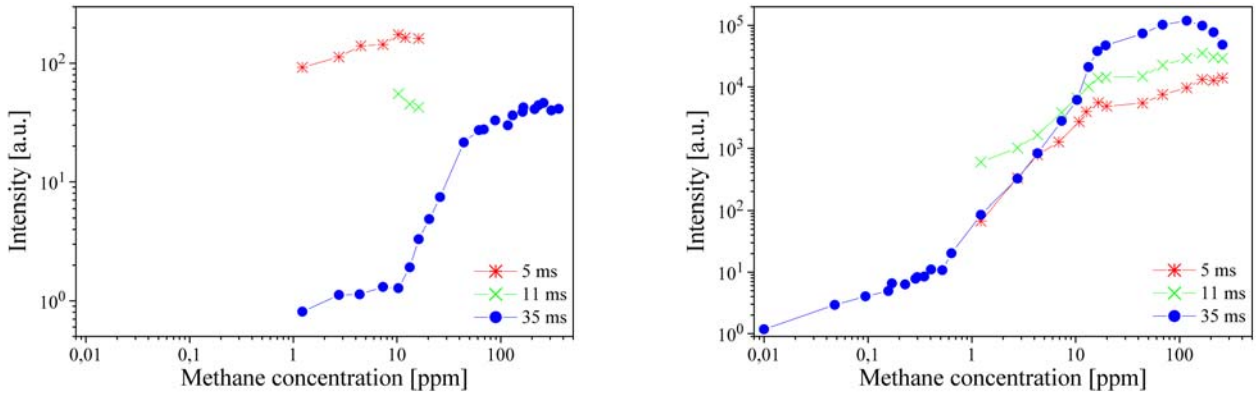

Fig. 28 The CN violet 7–7 band intensity as a function of the methane concentration at different decay times at wall temperatures of 300 K (left) and 77 K (right)

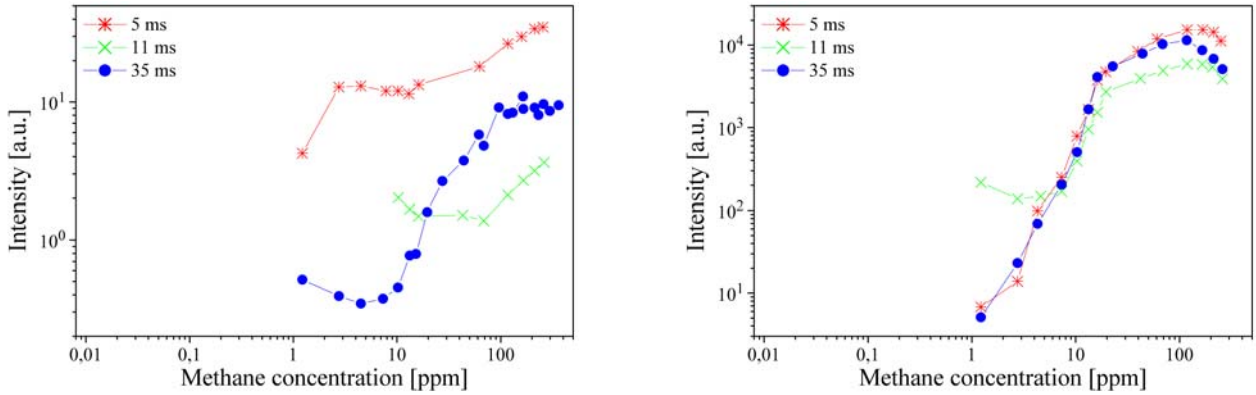

Fig. 29 The CN violet 12–12 band intensity as a function of the methane concentration at different decay times at wall temperatures of 300 K (left) and 77 K (right)

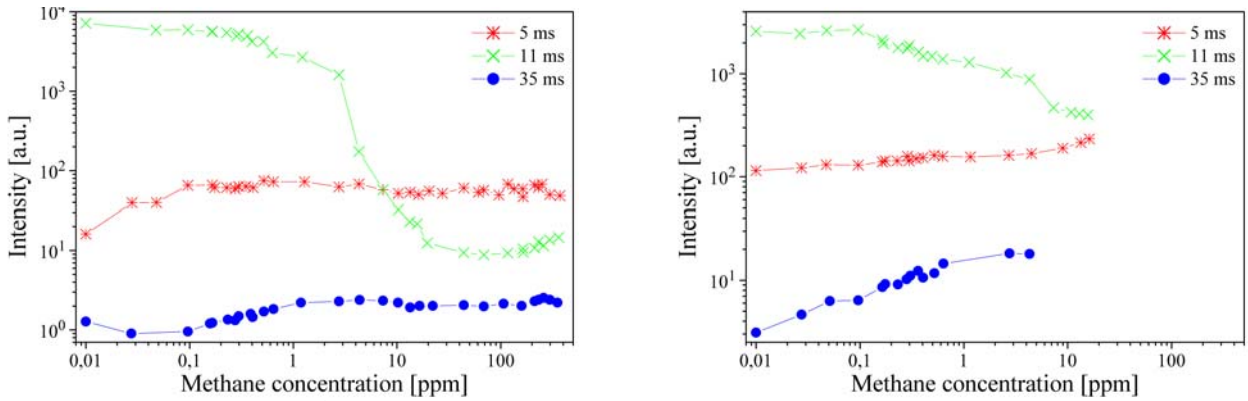

Fig. 30 The nitrogen 2nd pos. 1–3 band intensity as a function of the methane concentration at different decay times at temperatures of 300 K (left) and 77 K (right)

The dependencies obtained for CN violet 7–7 and 12–12 bands are presented in Fig. 28 – 29. All the graphs show an increase of the band intensities with an increase of the methane concentration. The saturation of the intensity and its following decrease can be seen at the low wall temperature at the highest methane concentrations, especially at the latest decay times. It is interesting that the intensities at the wall temperature of 77 K are more or less independent of the post-discharge position at the times later then the pink afterglow. The decreasing part of the dependencies in Fig. 29 measured in the pink afterglow results from the overlap of the studied band by the 2nd pos. 2–5 band that is strongly quenched in the pink afterglow.

Fig. 27 shows the combination of relations obtained for the 1st neg. and CN violet system. At the lowest methane concentrations the intensity of 1st neg. 1–1 is dominant, at the higher concentrations the intensity of CN 0–0 becomes dominant. The dominance of this second band increases with the

decrease of the wall temperature where the dependencies are more or less the same as the dependencies of the other CN violet bands.

Figure 30 presents the relations obtained for the 2nd pos. 1–3 band. The dependencies are similar to the dependencies obtained for the 1st neg. 0–0 band. The increase of the intensities at higher methane concentrations, especially at the low wall temperature, results from the overlap of this band by the extended rotational structure of the strong CN violet 0–0 band.

The experimental data obtained in the microwave post-discharge were strongly limited to one decay time and also the range of the studied methane concentration was not too wide. Due to these facts, the results are not presented here in the graphic form. The results obtained during these measurements show the same dependencies as in the DC post-discharge and also correlate with them well. A difference could be seen only in the intensity of the CN violet 7–7 band that is more intensive in the microwave post-discharge than in the DC afterglow because there is a higher dissociation degree in the microwave discharge and thus the recombination is also more effective.

6 NITROGEN AFTERGLOW WITH TRACES OF HALOGENATED HYDROCARBONS

The unexpected high intensity of CN violet and red spectral systems, especially at the low wall temperature, provide the application idea to use this high sensitivity in monitoring of the polymeric materials disintegration that is discussed in the next section. Many polymeric materials are based not only on pure hydrocarbons, but chlorinated and fluorinated hydrocarbons are usually also used (for example in PVC, Teflon, etc.). Due to these facts it is necessary to verify if the partially or fully halogenated hydrocarbon traces have the same or similar influence on the pure nitrogen afterglow.

The experimental studies were not as extensive as in the case of the methane traces. The optical emission spectra of the CN (violet and red systems) and nitrogen 1st pos., 2nd pos. and 1st neg. systems were measured at three decay times of the DC flowing post-discharge. The plasma was created at the total gas pressure of 2000 Pa (three times higher than before) and the discharge current was 125 mA. The impurity concentration in an active discharge was varied in the range of two orders only, using the laboratory prepared high pressure mixtures that were calibrated by the ICP spectroscopy. The chemical composition of the used admixtures is presented in the table 2 due to the fact that not all of the gases used are simple gases. Due to the ban of various halogenated hydrocarbons (known also as freons), common gases (or liquids) from refrigerating devices and liquids used in laboratory for cleaning were used for these studies. The optical spectra emitted during the afterglow were recorded at three decay times of about 29, 54 and 86 ms at the reactor wall temperatures of 77 K and 300 K.

Table 2: Halogenated hydrocarbons used in this study

Trade name	**Other names**	**Chemical composition**
dichlormethane	methylenchloride	CH_2Cl_2
trichlormethane	chloroform	$CHCl_3$
tetrachlormethane		CCl_4
dichlorethylene	perchlorethylene	$C_2H_2Cl_2$
R12		CHF_2Cl
R22		CF_2Cl_2
R134a		$C_2H_2Cl_4$
R413a	ISCEON49	88 % R134a + 9% R218 + 3% R600a
R218		C_3F_8
R600a	isobutane	C_4H_{10}

To eliminate the discharge instabilities and to reach the accuracy of the discharge conditions set-up, the ratio of the CN violet 0–0 band head intensity to the nitrogen 2nd pos. 1–3 band was calculated to obtain an objective indicator of the carbon presence. This procedure gives better results at lower

carbon concentrations when the nitrogen band has a sufficient intensity. At the high concentrations it is better to measure directly the CN violet 0–0 band intensities because the nitrogen band has only the small intensity near the noise level and thus the experimental error rapidly increases. The examples of the experimental results obtained using halogenated hydrocarbons are presented in Fig. 31. The results obtained in the nitrogen–methane gas mixture are added as a reference and these dependencies were re-measured at the new conditions described above. All the data are re-calculated on the concentration of atomic carbon in the discharge to obtain an objective value independent on the structure of the trace molecule. The figures show an excellent agreement among all the experimental data, no significant differences among the various admixtures can be seen. The observations of various molecular bands of the other spectral systems mentioned above do not show any deviations from the dependencies obtained in the nitrogen–methane mixture. It means the processes during the afterglow are not significantly changed by the halogen atoms presence. More or less the same results have been obtained also at the other positions during the post-discharge.

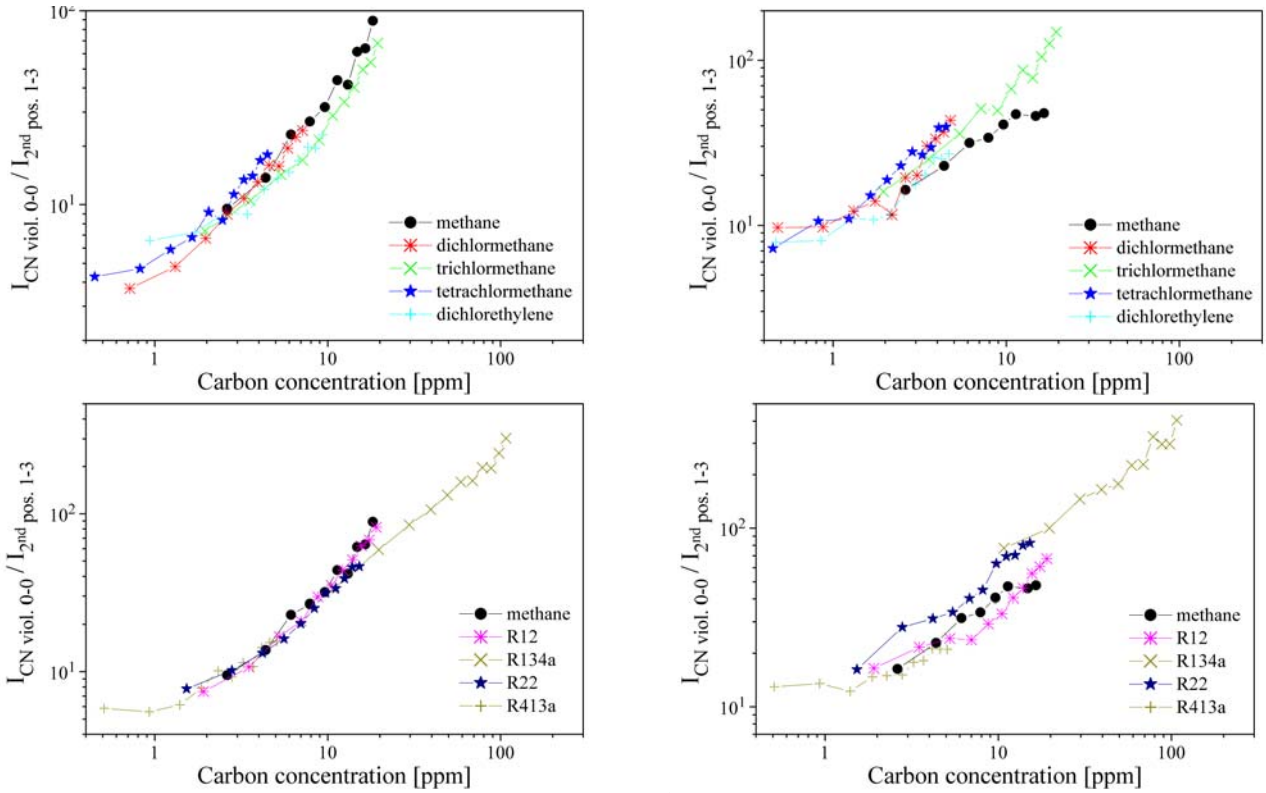

Fig. 31 CN violet 0–0 band head related to N_2 2^{nd} pos. 1–3 band head as a function of carbon atoms presence in discharge (decay time of 54 ms, wall temperature 300 K – left and 77 K – right)

7 APPLICATION IN THE MONITORING OF POLYMER MATERIAL DISINTEGRATION

On the basis of spectroscopic measurements presented in the previous sections, a new method for determination of a hydrocarbon concentration was proposed and consequently realized in practice. Later, it was simplified on the basis of an integral measurement of intensity of the optical emission spectrum by a semiconductor photodetector in the nitrogen afterglow at a low temperature. The advantage of the proposed method is its technical simplicity and economy of the measuring equipment. The method including its simplified variant and some results obtained by it are presented in this section.

7.1 THE PRINCIPLE AND TECHNICAL BACKGROUND OF THE METHOD

The method uses an optical spectrometer with a resolution better than 0.1 nm coupled with any multichannel detector (PDA or CCD) as a monitor of the afterglow emission at a low wall temperature. By the procedure given in the last section the CN violet 0–0 band head intensity is compared with the head intensity of 2^{nd} pos. 1–3 band. In the case of CN the most intense band is used (this is valid in DC afterglow, when the microwave discharge is used as a plasma source, the 7–7 band intensity is higher or the same as it was said before). Use of the 2^{nd} pos. 0–2 band which is more intense and which is closer to the CN violet bands is not recommended due to the fact that his band may be at higher carbon concentrations overlapped by a rotational structure of CN violet bands and it can be overlapped by the 0–11 band of NO^{β} system if oxygen traces are present.

The method is very sensitive (with the detection limit of order 0.01 ppm of atomic carbon) but rather expensive for wide use. On the basis of detailed studies of the afterglow in nitrogen with various hydrocarbon traces a new procedure for estimating the carbon traces in nitrogen [19] was proposed. Due to the fact that the nitrogen positive spectral systems are almost independent of the methane presence it is possible to measure the light emission in an integral form. The contribution of nitrogen radiation will be almost independent of the carbon presence. The changes corresponding to CN radiation are more than three orders higher then changes in the nitrogen band intensities and as it was shown before these changes are stronger at lower temperature. The emission of the CN violet system is the most sensitive one to the hydrocarbon presence therefore we use an optical band filter (with a passing range in the zero sequence of CN violet system wavelength interval) to eliminate the other influences. We measured simultaneously the integral spectrum of the afterglow at a higher temperature to eliminate any discharge fluctuations and also to compensate the slight dependence of the nitrogen emission on methane traces.

Both measurements were done with the same type of light detector. Due to an insufficient sensitivity of the light detectors in the UV range and due to a low intensity of the emitted light the direct measurement of the detector signal could not be used. Thus we used the synchronous detection method. The ratio of both channel values can be used for an estimation of the carbon concentration after elimination of all disturbing influences by the combination of analogue and digital processing of the signal.

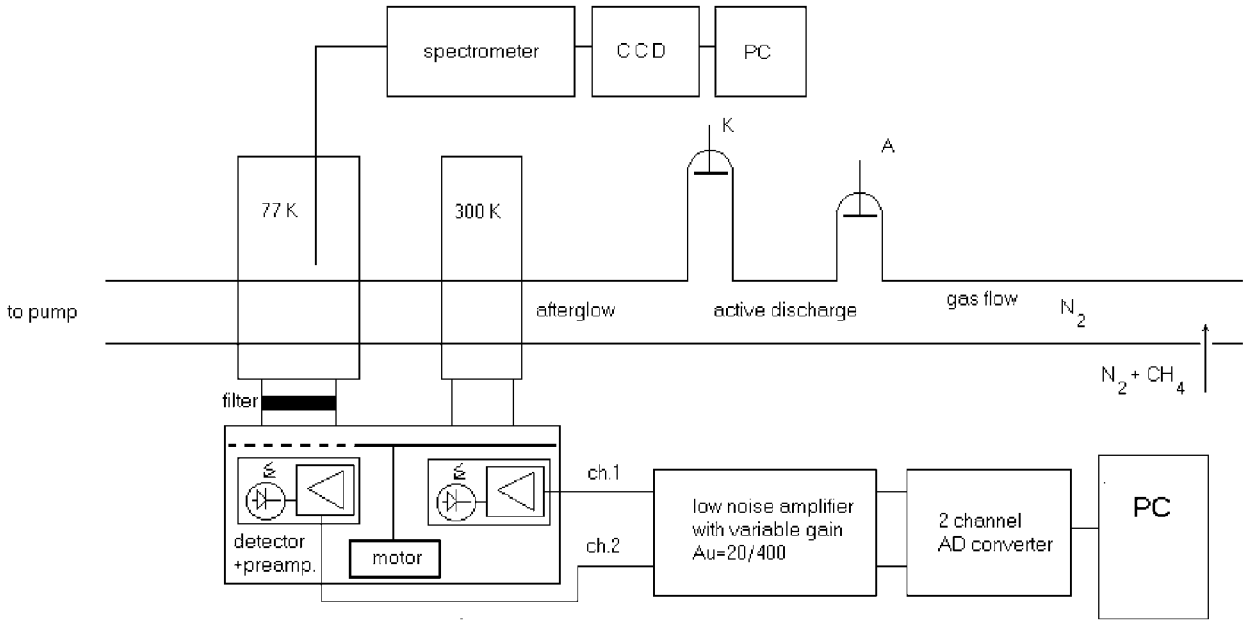

Fig. 32 The scheme of the experimental setup

The experimental device was derived from the setup presented in Fig. 1 where a simple measuring equipment was applied simultaneously with the common optical emission spectroscopy. The schema is shown in Fig. 32. Two optically isolated boxes were placed around the discharge tube at the afterglow times of 24 and 30 ms. The first one was used for measuring the integral spectrum in the whole detector sensitivity range at the ambient wall temperature, the second one was equipped by an optical filter (the passing range of 387 ± 13 nm, i.e. in the range of zero sequence of the CN violet system as we proposed above) and it could be immersed down to the temperature of liquid nitrogen.

To measure the emitted light, an electrically and optically shielded chamber containing a mechanical chopper was located at both boxes. Two independent blocks of detectors with low-noise preamplifiers were located behind the chopper to measure the light intensity from each box separately. The planar silicon PIN photodiodes BPW34B [70] with increased blue sensitivity were used as light detectors. The outputs of the detectors were connected to the amplifiers with a variable gain (A_u = 20 or 400). The next processing was done by a 12-bit AD converter controlled by a PC. The chopper driven by an asynchronous motor used the chopping frequency of about 300 Hz. The gain of the amplifiers was adjusted to avoid the saturation of the AD converters and these values were also controlled by a PC.

Thanks to the designed experimental setup and the numerical processing of the data the complicated system of analogue synchronous detection can be avoided. Due to this fact we did not need the reference signal from the chopper, which would have had a disturbing influence on the output signal from the detectors. For each measurement, 5000 samples were obtained by the AD conversion, then an FFT [62] was made; the signal amplitude around the chopping frequency i.e. 300 ± 5 Hz was obtained as the result detector value. Thus we have eliminated the noise of the detector and the other disturbing components of the signal and the influence of an inaccuracy caused by fluctuations of the chopper speed. The result value was then divided by the gain of the amplifier so that it would be proportional to the intensity of the optical radiation. Finally we calculated the ratio of the signal from the cooled part of the discharge tube to the reference integral signal to characterize the CN radical presence.

7.2 PROPERTIES OF THE METHOD

The experiment was realized for several different ranges of methane concentration. The photodetector measurement was simultaneously completed by an optical emission spectroscopy measurement. There were two main purposes of the experiment: the first one was to confirm the possibility of avoiding the expensive spectroscopic measurement by using an integral detector with an interference filter instead, the second purpose was the equipment calibration, i.e. the estimation of the dependence of the output value on the methane impurity concentration.

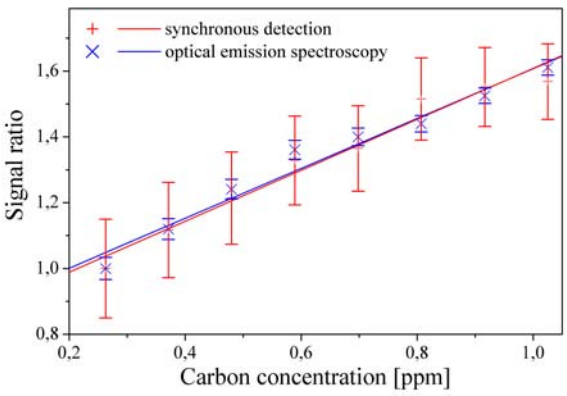

Fig. 33 A comparison of the simplified met-hod with the optical emission spectroscopy

The dependence of the detector voltage of both channels (channel 1 with a band-pass filter at 387 nm and channel 2 without the filter) on the admixture concentration shows the channel 1 value with the filter was rising faster than the value of channel 2 with an increase of the methane concentration in the discharge. Both these values, of course, depend on the parameters of the experimental setup (the distance from the discharge tube and the other geometrical parameters, area of the detector, the discharge conditions etc.).

To eliminate this dependence, the ratio of the signals for the calibration of the measuring equipment was chosen for this purpose. The linear dependence was fitted to the experimental values with a good agreement with experimental data.

The spectroscopic measurement and the measurement with the photodetector were compared. It was necessary to confirm the applicability of the proposed method and to find out the sensitivity of the device for low methane concentrations. The calibration curve of both measuring methods is shown in Fig. 33.

7.3 A PRACTICAL APPLICATION

Both described methods were simultaneously used for the determination of polyhydrocarbon materials destruction under low pressure at ambient sample temperature. The polymeric sample was placed into the reactor 40 cm in front of the beginning of an active discharge to minimize the UV discharge radiation (see Fig. 1). To determine the time evaluation of the material destruction both methods were used at proposed conditions. The polyethylene (surface area of 45 cm^2) and polypropylene (32 cm^2) tubes were used as the testing samples. The reactor with the sample was being evacuated for 30 minutes by a rotary oil pump coupled with a double liquid nitrogen trap and thereafter under normal operating conditions the reactor was partially cleaned to remove the molecules adsorbed on the reactor walls. We used the total gas pressure of 1000 Pa to increase the concentration of vibrationally excited nitrogen molecules (to increase the sensitivity of the method, see below) and the observations have been realized at the decay time of 30 ms. The signals obtained by both methods were recalculated using the calibration curve shown in Fig. 33 to estimate the carbon concentration equivalent and thereafter the value was related to the 1 m^2 of the sample surface. These experimental results as they developed during one hour are given in Fig. 34.

The experimental curves obtained by both methods are very similar and they can be approximated by a double exponential function. The faster decay probably corresponds with the desorption of hydrocarbon molecules adsorbed on the sample surface and reactor walls, the second decay coefficient could represent the pure destruction rate of the polymeric sample. These effects could be subjects of future studies.

The simple method for determination of polyhydrocarbon materials destruction was tested also by other polymeric samples including PVC and Teflon with similar results as we described for polyethylene and polypropylene. Thus this simple method could be applied in packing and food industries as a simple monitor of material stability.

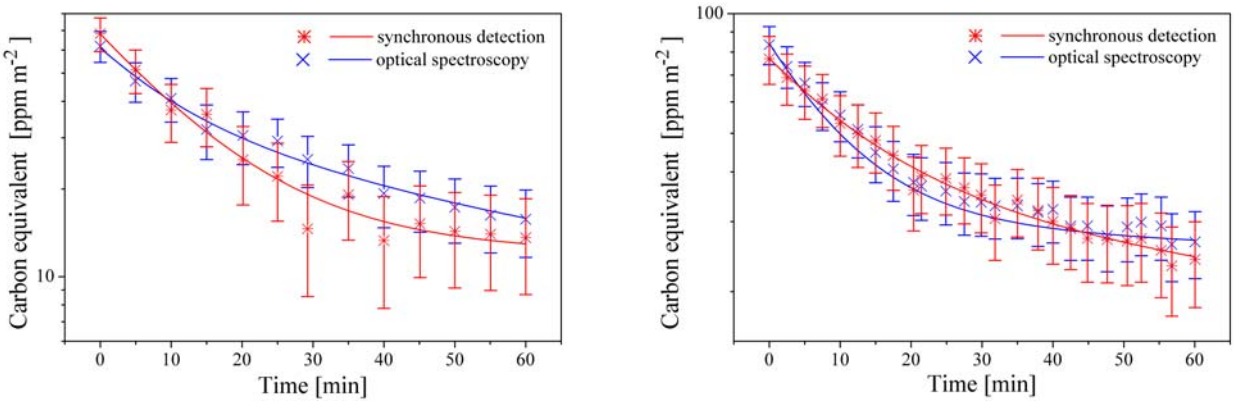

Fig. 34 Decay of polyethylene (left) polypropylene (right) samples measured by both data processing methods

8 MAIN KINETIC PROCESSES DURING THE AFTERGLOW OF NITROGEN AND ITS MIXTURES WITH HALOGENATED HYDROCARBONS

For modeling of the plasma processes, it is necessary to know the macroscopic plasma parameters (electric field, dimensions of device, total gas pressure, etc.) as well as the coefficients of collisional processes and diffusion for all electronic-vibrational molecular states. The macroscopic parameters have been given in section describing the experimental devices. This section describes the microscopic processes in plasma.

In plasma, four different groups of processes can be observed. During the active discharge at low pressures, the collisions of electrons with heavy particles are dominant, as well as the radiation. The collisions among heavy particles (and the collisions with the walls of a plasma reactor) play a dominant role during the afterglow. The fourth process, diffusion, plays the significant role during both previous cases, especially at low pressures.

The electronic collisions are usually characterized by cross-sections in dependence on the incident electron energies. These values have been reviewed for nitrogen by [9, 75, 50] and thus they are not presented here. The values for the methane and halogenated hydrocarbons and their various fractions no complex review exists at this moment and the data must be selected from more bibliographic sources as [75, 43, 12].

The nitrogen radiative processes have been reviewed by [38, 13], the complex data of CN radiations are not available but some reports have been published [60, 61, 63] for the main CN spectral systems ($A\ ^2\Pi \rightarrow X\ ^2\Sigma^+$ and $B\ ^2\Sigma^+ \rightarrow X\ ^2\Sigma^+$). For the other CN spectral systems, some band positions are available in tables [49] but no data are available for the transition probabilities.

The diffusion coefficients are known for some metastable atomic and molecular states [81, 10, 39, 4, 41]. The diffusion of the non-metastable molecular states was not measured because it does not play any significant role.

The problems of the heavy particle collisions has not been reviewed up to this moment though many state specific coefficients are described in literature. The huge review of these state selective processes, mostly with the rate constants, have been given in [30] for pure nitrogen and nitrogen–methane mixture, the review of the kinetic processes of plasma created in the air–methane mixture [44] has been published, too.

The next subsection concludes the mechanisms of three main heavy particle collisional processes observed during the post-discharge. The following subsections give very simple stationary models of the populations of the electronic states, from which the radiative transitions have been observed during this work.

8.1 MECHANISMS OF THE MAIN HEAVY PARTICLE COLLISIONAL PROCESSES

8.1.1 Recombination of atoms

Atomic recombination is known for many years. The first models of this process have been created for the pure nitrogen in 1956 [5]. In 1988, a very accurate theory of the two ground state nitrogen atoms recombination has been given [48] and later confirmed also by the experimental works [55]. The N ($^4S_0$) atoms (atoms in their ground state) can by recombination form directly only N_2 ($X\ ^1\Sigma_g^+$), N_2 ($A\ ^3\Sigma_u^+$), N_2 ($A'\ ^5\Sigma_g^+$) and N_2 ($^7\Sigma_u^+$) molecular states, thus one of them must be a precursor state for N_2 ($B\ ^3\Pi_g$) formation. The N_2 ($^7\Sigma_u^+$) state is repulsive [47] and the N_2 ($X\ ^1\Sigma_g^+$) state does not lay close to N_2 ($B\ ^3\Pi_g$) state in appropriate energy ranges, hence these two state can not play the role of precursors. It was shown [48] that the N_2 ($A'\ ^5\Sigma_g^+$) state is the precursor [48].

The recombination of the N ($^4S_0$) and N ($^2D_0$) atoms is known [74, 42, 77, 27], too, but the appropriate model of this reaction mechanism has not been given. It is known that during this inverse predissociation reaction, the N_2 ($C''\ ^5\Pi_u$) state plays the precursor role. This state has only one potential minimum, no outer Van der Waals minimum as in the N_2 ($A'\ ^5\Sigma_g^+$) state case has been

observed. The study of this recombination reaction is relatively difficult, because the concentration of the N ($^2D_0$) state is about two orders lower than the N ($^4S_0$) concentration and the influence of the energy pooling (see later) thus plays more important role. At low temperature (77 K) the enhancement of the band intensities originating from the N_2 (C $^3\Pi_u$, $v = 4$) level has been observed [74]. This level lays just bellow the predissociation limit of N_2 (C $^3\Pi_u$) state, thus the interpretation of this effect could be probably similar as in the case of N_2 (B $^3\Pi_g$, $v = 12$) level.

For recombination of the N ($^4S_0$) and C (^3P) atoms many data are not available, either. The reaction scheme could be following:

N ($^4S_0$) + C (^3P) + M → CN (B $^2\Sigma^+$, $v = 7$) + M

where M is the third body. Any precursor state must exist for the CN (B $^2\Sigma^+$) state population, due to the fact that the ground state atoms can form only the CN (X $^2\Sigma^+$), CN (A $^2\Pi$), CN (C $^4\Sigma^+$), CN (X $^4\Pi$) stable states and two sextet repulsive states. The interactions among the first three states are well known [20, 45, 79, 80, 30], but they are not specified enough for strong overpopulation observed on the CN (B $^2\Sigma^+$, $v = 7$) level. It was proposed [79] that the CN (B $^2\Sigma^+$, $v = 7$) level could be populated by quenching of the CN (C $^4\Sigma^+$) state, which is created directly by the atomic recombination. On the other hand, the inverse predissociation into the CN (E $^2\Sigma^+$) and CN (F $^2\Delta$) states can be significant, too. Thus the further observations are necessary for the appropriate description of the CN creation by atomic recombination.

The recombination reactions described above are three body reactions. Except for them, the two body recombination reaction are observed, too, and at the lowest pressures they are dominant. The following reactions have been observed [2, 76]:

N ($^4S_0$) + N ($^4S_0$) → N_2 (B $^3\Pi_g$, $v = 13$)

N ($^4S_0$) + N ($^4S_0$) → N_2 (a $^1\Pi_g$, $v = 6$)

Any other reactions are possible, but those reactions are not described in literature. At experimental conditions of the presented work, these two body recombinations probably do not play any significant role. Due to this fact it is not necessary to study them in closer detail. The wall processes play also significant role in the recombination problem. These processes are dependent on the wall material and the molecules are formed also preferentially in some vibrational states similar to the three body recombination. Some rate coefficient data can be found in [7, 41].

8.1.2 Energy pooling

The term energy pooling reaction means the collision of two excited molecules (vibrationally or electronically). During this collision the excitation energy of one molecule is transferred into the other molecule. A typical example of such reaction is so called triplet-triplet annihilation:

N_2 (A $^3\Sigma_u^+$) + N_2 (A $^3\Sigma_u^+$) → N_2 (X $^1\Sigma_g^+$) + N_2 (C $^3\Pi_u$)

Although this reaction is known for many years [72], the mechanism of this type of reactions has been given recently [56] when the isotopically marked $^{15}N_2$ (X $^1\Sigma_g^+$, $v \geq 4$) molecules with the $^{14}N_2$ (A $^3\Sigma_u^+$) state has been used. The results show that the excitation energy is transferred from the higher excited state to the other state. The energy pooling reactions play significant role during the nitrogen afterglow in the population of the N_2 (B $^3\Pi_g$), N_2 (C $^3\Pi_u$) and N_2 (C" $^5\Pi_u$) states. This type of reaction contributes to population of the other nitrogen states, too, but the observations of such processes are not carried too often.

For the evaluation of the reaction coefficient, the Frank-Condon model associated with minimum-energy-defect model can be used [52]. By this model, the reaction coefficient can be computed by formula $k = q_1 \cdot q_2 \cdot \exp(|\Delta E|/kT)$ where q_1 and q_2 are the Frank-Condon factors for transition of the first and second interacting molecule, respectively, $|\Delta E|$ is the magnitude of the energy defect in the energy transfer reaction and kT have the usual meaning.

8.1.3 Energy transfer reactions between the near laying states

This group of reactions includes reactions between near laying vibrational levels, for example
CN ($A\ ^2\Pi$, $v = 10$) + M → CN ($B\ ^2\Sigma^+$, $v = 0$) + M

Although these resonance transitions are intense studied but the rate coefficients of these excitation energy transfers are established only in a few cases.

The vibrational coupling of the nitrogen triplet states ($N_2(A\ ^3\Sigma_u^+)$, $N_2(B\ ^3\Pi_g)$, $N_2(W\ ^3\Delta_u)$ and $N_2(B'\ ^3\Sigma_u^-)$ states) is a very well described system [8, 1, 36]. The other well known system includes nitrogen singlets N_2 ($a\ ^1\Pi_g$), N_2 ($a'\ ^1\Sigma_u^-$) and N_2 ($w\ ^1\Delta_u$) [40, 25]. For the other couplings in nitrogen, many references are not available, especially those including the rate constants or cross-sections. Many vibrational couplings are well known and studied also in the CN radical, but the quantification of these processes has not been measured directly. The rate coefficients can be predetermined by the minimum-energy-defect model, but such an estimation will probably have a great error and it can be used for the first estimation only.

8.2 POPULATION MECHANISMS OF $N_2(B\ ^3\Pi_g)$, $N_2(C\ ^3\Pi_u)$, $N_2^+(B\ ^2\Sigma_u^+)$ AND CN ($B\ ^2\Sigma^+$) AND CN ($A\ ^2\Pi$) STATES

The main population and depopulation mechanisms of the studied molecular states in stationary state are listed separately for each of the studied state. Many kinetic reactions and their rate coefficients are known (see review in [30]) but also a huge number of the processes is not fully described, the reaction constants are missing and also some reactions are actually unknown. Due to these facts, only the main reaction channels are included in the population and depopulation processes and the vibrational specification is not used in many cases, because the model presented here should be considered as the first approximation. For more exact model it is possible to study every vibrational level separately and in time evolution, but it is not the subject of presented study. The appropriate models were developed for example in Prague [35] and Lisbon [68, 15, 16].

The population balances presented in the following paragraphs are given for the afterglow conditions. Thus the excitation caused by collisions with electrons is neglected, because the characteristic time for the electron thermalization is in order of a few microseconds, but the afterglow was studied at decay times in orders of milliseconds. The concentrations of the atomic and molecular states in the discharge and during the post-discharge are not known. For the exact study they could be computed from the active discharge conditions. Due to this fact the approximated values in the active discharge (based on [59, 10, 57]) have been used for the prediction of the population balances presented bellow. As fare as the other molecular states are concerned, the appropriate data are not available, thus the processes including these states will be estimated where it will be necessary.

8.2.1 Population balance of the $N_2(B\ ^3\Pi_g)$ state

The reactions included in the simple model are following:

R1	$N_2(X\ ^1\Sigma_g^+, v \geq 14) + N_2(X\ ^1\Sigma_g^+, v \geq 14) \rightarrow N_2(B\ ^3\Pi_g) + N_2$	$k_1 = 10^{-15}\ cm^3 \cdot s^{-1}$	[71]
R2	$N_2(X\ ^1\Sigma_g^+, v \geq 4) + N_2(A\ ^3\Sigma_u^+, v) \rightarrow N_2(B\ ^3\Pi_g) + N_2$	$k_2 = 4 \cdot 10^{-11}\ cm^3 \cdot s^{-1}$	[56]
R3	$N_2(A\ ^3\Sigma_u^+) + N_2(A\ ^3\Sigma_u^+) \rightarrow N_2(B\ ^3\Pi_g) + N_2$	$k_3 = 3 \cdot 10^{-11}\ cm^3 \cdot s^{-1}$	[71]
R4	$N(^4S_0) + N(^4S_0) + N_2 \rightarrow N_2(B\ ^3\Pi_g) + N_2$	$k_4 = 6 \cdot 10^{-33}\ cm^6 \cdot s^{-1}$	[64]
R5	$N_2(C\ ^3\Pi_u) \rightarrow N_2(B\ ^3\Pi_g) + h\nu$	$k_5 = 3 \cdot 10^7\ s^{-1}$	[13]
R6	$N_2 + N_2(B\ ^3\Pi_g) \rightarrow N_2 + N_2$	$k_6 = 2 \cdot 10^{-11}\ cm^3 \cdot s^{-1}$	[55]
R7	$N_2(B\ ^3\Pi_g, v) \rightarrow N_2(A\ ^3\Sigma_u^+) + h\nu$	$k_7 = 10^6\ s^{-1}$	[13]

The $N_2(B\ ^3\Pi_g)$ state (the upper state of the 1st pos. emission) is dominantly populated by the energy pooling reactions R1 – R3 of the both lower laying metastable states (N_2 ($X\ ^1\Sigma_g^+$) and $N_2(A\ ^3\Sigma_u^+)$. The three body recombination (reaction R4) contributes significantly to the population on higher vibrational levels ($v = 10 – 12$), especially in the later afterglow. The strong collisional bounds with the other nitrogen triplet states are not negligible, either, but the appropriate data for computing

their contribution are not available. The 2nd pos. emission (radiative transition from $N_2(C\ ^3\Pi_u)$ state, reaction R5) contributes to the $N_2(B\ ^3\Pi_g)$ population, too.

In the depopulation of the $N_2(B\ ^3\Pi_g)$ state, two main processes can be observed. The first of them is the nitrogen 1st pos. system emission (R7), the second one is the collisional quenching by other molecules (R6). Calculating the balance equation using the vibrationally excited states concentrations given by [59, 10, 57] can be seen that the pooling of one ground state molecule with a molecule excited into the $N_2(A\ ^3\Sigma_u^+)$ state is the dominant population process and that the contribution of the radiative transition from the $N_2(C\ ^3\Pi_u)$ state is not negligible. The other processes are not significant in modeling this state in complex. In the depopulation both proposed processes are of the same order, thus none of them can be neglected.

This model is valid for the vibrational level under the predissociation limit at level $v = 12$. The experiments showed also some transition from the levels over this limit. No accurate data are available. The recombination as well as the emission of 2nd pos. system could not contribute to the population. Thus the pooling and coupling with the other triplet states must be dominant processes.

The populations on levels just above the predissociation limit ($v = 13 – 15$) are relatively small even in the pink afterglow where they can be directly populated also by electrons. Due to this fact the population minima at these levels are not so low as in later afterglow. The higher levels ($v = 16 – 20$) are probably populated by some energy pooling reactions of lower states. This explanation is based on similarity between the slope of dependence of population on the decay time and the lowest levels which are populated by this mechanism [53, 54, 55]. At higher wall temperatures, the maximum of population among these levels can be seen at levels $v = 17$ and 18, but at lower temperatures the population at level $v = 17$ dominates thus the exciting reaction has a resonance character. The list of possible energy transfer reaction have been given in [32].

Except the pooling reactions, the vibrational coupling of the nitrogen triplet states can contri-bute to the $N_2(B\ ^3\Pi_g)$ population. It can be concluded, that the collisional transfer of the excitation energy is dominantly significant for $N_2(B\ ^3\Pi_g)$ levels 17 and 18, even at low temperatures.

8.2.2 Population balance of the $N_2(C\ ^3\Pi_u)$ state

This state can be populated by different pooling reactions as well as by nitrogen atoms recombination. The radiative transitions from the upper states do not play any significant role. The process of the electron–ion recombination, which can populate this state, too, is not included as well as the coupling with the other triplet states laying near the $N_2(C\ ^3\Pi_u)$ state.

R5	$N_2(C\ ^3\Pi_u) \rightarrow N_2(B\ ^3\Pi_g) + h\nu$	$k_5 = 3 \cdot 10^7\ s^{-1}$	[13]
R8	$2 \cdot N_2(X\ ^1\Sigma_g^+, v \geq 24) \rightarrow N_2(X\ ^1\Sigma_g^+) + N_2(C\ ^3\Pi_u)$	$k_8 = 3 \cdot 10^{-10}\ cm^3 \cdot s^{-1}$	[71]
R9	$N_2(X\ ^1\Sigma_g^+, v \geq 19) + N_2(A\ ^3\Sigma_u^+) \rightarrow N_2 + N_2(C\ ^3\Pi_u)$	$k_9 = 3 \cdot 10^{-10}\ cm^3 \cdot s^{-1}$	[71]
R10	$N_2(A\ ^3\Sigma_u^+) + N_2(A\ ^3\Sigma_u^+) \rightarrow N_2(X\ ^1\Sigma_g^+) + N_2(C\ ^3\Pi_u)$	$k_{10} = 1.5 \cdot 10^{-10}\ cm^3 \cdot s^{-1}$	[52]
R11	$N_2(A\ ^3\Sigma_u^+) + N_2(B\ ^3\Pi_g) \rightarrow N_2(X\ ^1\Sigma_g^+) + N_2(C\ ^3\Pi_u)$	$k_{11} = 4.6 \cdot 10^{-10}\ cm^3 \cdot s^{-1}$	[57]
R12	$N(^4S_0) + N(^2D_0) + N_2 \rightarrow N_2 + N_2(C\ ^3\Pi_u)$	$k_{12} = 10^{-33}\ cm^6 \cdot s^{-1}$	[27]
R13	$N_2 + N_2(C\ ^3\Pi_u) \rightarrow N_2 + N_2$	$k_{13} = 10^{-11}\ cm^3 \cdot s^{-1}$	[71]

Two processes can be observed also in the depopulation – the radiative emission of the 2nd pos. system and the quenching by other molecules.

From the balance equation was obtained result that the pooling of two lowest electronic states plays dominant role and the recombination of the nitrogen atoms can be neglected. The $N_2(C\ ^3\Pi_u)$ state quenching can be neglected due to the short radiative lifetime of this state. The light emission is the main depopulating process. The other metastable states can significantly contribute to the $N_2(C\ ^3\Pi_u)$ population, but their role is not fully understood.

8.2.3 Population balance of the N_2^+ ($B\ ^2\Sigma_u^+$) state

The problem of this molecular state population mechanisms is much more complicated in comparison with the other states. Two different processes must be separated. The formation of the nitrogen molecular ion is the first one, the second one is excitation this ion.

R14 $N_2\ (X\ ^1\Sigma_g^+,\ v \geq 12) + N_2^+\ (X\ ^2\Sigma_g^+) \rightarrow N_2\ (X\ ^1\Sigma_g^+) + N_2^+\ (B\ ^2\Sigma_u^+)$ $k_{14} = 5 \cdot 10^{-10}\ cm^3 \cdot s^{-1}$ [16]

R15 $N_2^+\ (B\ ^2\Sigma_u^+) \rightarrow N_2^+\ (X\ ^2\Sigma_g^+) + h\nu$ $k_{15} = 3 \cdot 10^7\ s^{-1}$ [13]

R16 $N_2 + N_2^+\ (B\ ^2\Sigma_u^+) \rightarrow N_2 + N_2^+$ $k_{16} = 3.4 \cdot 10^{-10}\ cm^3 \cdot s^{-1}$ [71]

The nitrogen molecular ion formation results from the stepwise ionization processes [59] or by the collisions of various highly excited neutral metastable states then their excitation energies are coupled and thus the secondary ionization can be observed. Of course, the electron ion recombination decreases the molecular ion concentration. This process is much slower then creation in the earlier post-discharge where high concentrations of metastable neutral species can be observed. During the later afterglow the ion concentration decreases due to the recombination as well as due to the fact that the vibrationally excited nitrogen ground state concentration is decreased by the other processes.

The N_2^+ ($B\ ^2\Sigma_u^+$) state, after its creation, is dominantly populated by an excitation of the molecular ion ground state N_2^+ ($X\ ^2\Sigma_g^+$) by collisions with vibrationally excited nitrogen neutral molecules (reaction R14). The direct ionization collisions of the highly excited neutral molecules can contribute to N_2^+ ($B\ ^2\Sigma_u^+$) population, too, but these reactions have not been up to now studied well enough and so it is difficult to include such processes into the model. The influence of the collisionally induced dissociation of the nitrogen clusters could be hardly included into the model correctly due to the fact that their concentrations are not known and now they can not be estimated from any other experiments, either. The radiative transitions from the higher excited states do not play any significant role and they can be neglected. In the depopulation, both the radiation and quenching processes are included. The losses by the electron–ion recombination are not included in this first approximation model, either because the concentration of electrons is at the post-discharge conditions relatively low.

From the above is evident, the main populating process of the N_2^+ ($B\ ^2\Sigma_u^+$) state is the excitation transfer from the vibrationally excited ground state of the neutral nitrogen molecule to the ground state of the molecular ion (see Fig. 35).

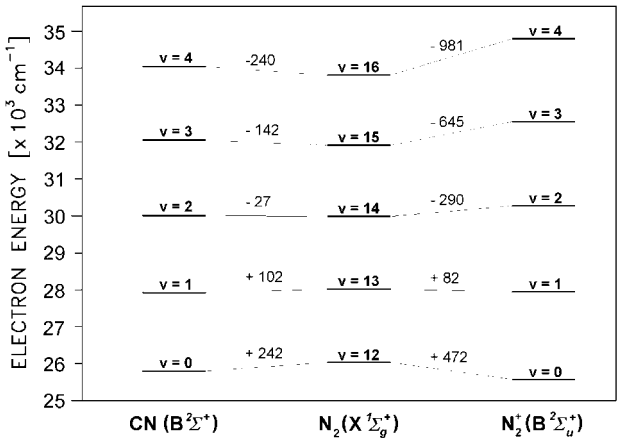

Fig. 35 Possible collisional induced energy transfers among the N_2 ($X\ ^1\Sigma_g^+$, v), N_2^+ ($B\ ^2\Sigma_u^+$, v') and CN ($B\ ^2\Sigma^+$, v'') states

The contribution of the other populating processes is by about two orders smaller. This is in accordance with older observations [77]. During the pink afterglow, when the emission of the 1st neg. system becomes stronger and also, a strong enhancement of electron concentration is observed, these additional processes probably start to play a more important role. In the depopulation, both processes have almost roughly the same efficiency. The computed value of the N_2^+ ($B\ ^2\Sigma_u^+$) concentration is 10^8 cm^{-3}. This is about 1 % of the total molecular ion concentration and it is in accordance with the predicted value.

8.2.4 Population balance of the CN ($A\ ^2\Pi$) state

The contribution of the N ($^4S_0$) and C (^3P) atomic recombination to the CN ($A\ ^2\Pi$, $v = 4 – 9$) that were observed in the experiment can be neglected due to very low concentration of the C (^3P) atoms in the post-discharge in our case. In addition, the recombination populates dominantly the levels just

under the dissociation or predissociation limit (especially at low temperature) which corresponds to the CN (A $^2\Pi$, v = 20) vibrational level; too high then the studied vibrational levels.

Some bands of the CN infrared system (CN (B $^2\Sigma^+$) → CN (A $^2\Pi$)) has been obser-ved but their intensities were by about 2 orders lower then spectra of the CN violet and red systems. Thus the light emission from the higher CN electronic states doesn't enable for the CN (A $^2\Pi$) populations to occur high enough for such intense CN red spectra as we observed. Due to these facts, only the collisional induced transfer of excitation energy can be sufficiently efficient populating process. The vibrational levels of the CN (A $^2\Pi$) state are of relatively low energy.

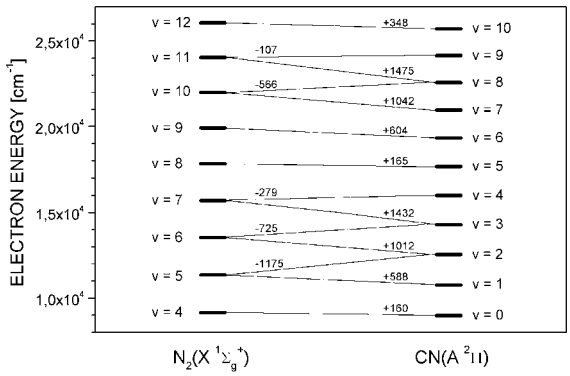

Fig. 36 Possible collisional induced energy transfers between the N_2 (X $^1\Sigma_g^+$, v') and CN (A $^2\Pi$, v'') states

Thus only vibrationally excited ground state nitrogen and CN molecules can play a role of precursor for CN (A $^2\Pi$) population. The carbon concentration in the discharge is at the maximum by about 4 orders lower then concentration of nitrogen and thus the first of the processes mentioned above can be an excitation energy source and it can be described by the reaction R17.

R17 N_2 (X $^1\Sigma_g^+$, $v \geq 4$) + CN (X $^2\Sigma^+$) → N_2 (X $^1\Sigma_g^+$) + CN (A $^2\Pi$, v) k_{17} = unknown [67]

R18 CN (A $^2\Pi$) → CN (X $^2\Sigma^+$) + hν $k_{18} = 10^7$ s^{-1} [61]

The possible transfers for selected CN (A $^2\Pi$) vibrational levels are given in Fig. 36. The energies of the vibrational levels have been calculated from classical formulas given in [17, 29] using the molecular constants given by [38] for nitrogen and by [61] for CN radical.

Due to the v–v processes in the nitrogen the initial Boltzmann vibrational distribution of the N_2 (X $^1\Sigma_g^+$) state transfers into well-known Treanor-Gordiets distribution where the population is inverse. This could explain the population inverse in the CN (A $^2\Pi$) state as it was observed.

8.2.5 Population balance of the CN (B $^2\Sigma^+$) state

For the modeling of this state population only a few accurate data are available. The excitation transfers from the nitrogen molecules as in the case of CN (A $^2\Pi$) state are dominant in the population. Due to many vibrationally resonances the excitation transfer between different states of the CN molecule is not probably negligible, either, but the rate coefficients or the cross-sections for these reactions have not yet been published. The contribution of recombination plays probably a significant role, especially at low temperatures. The CN (B $^2\Sigma^+$) state is depopulated mainly by the radiative emission. The quenching of this state by the nitrogen molecules is small. Due to these facts, the appropriate form of the balance equation can not be designed and the processes must be studied separately. The main process populating the CN (B $^2\Sigma^+$) state is the transfer of the excitation energy from the N_2 molecules described by the following reactions R19 and R20 (in the reaction R20, N_2^* means the electronically excited nitrogen molecule).

R19 N_2 (X $^1\Sigma_g^+$, $v \geq 12$) + CN (X $^2\Sigma^+$) → N_2 (X $^1\Sigma_g^+$) + CN (B $^2\Sigma^+$, v) $k_{19} = 1.2 \cdot 10^{-11}$ cm$^3\cdot$ s^{-1} [19]

R20 N_2^* + CN (X $^2\Sigma^+$) → N_2 + CN (B $^2\Sigma^+$) k_{20} = unknown [73]

R21 CN (B $^2\Sigma^+$) → CN (X $^2\Sigma^+$) + hν $k_{21} = 2 \cdot 10^7$ s^{-1} [61]

R22 N ($^4S_0$) + C (^{3}P) + M → CN (B $^2\Sigma^+$, v = 7) + N_2 $k_{22} = 9.4 \cdot 10^{-33}$ cm$^6\cdot$ s^{-1} [66]

R23 N + CN → N_2 + C $k_{23} = 10^{-10}$ cm$^3\cdot$ s^{-1} [65]

As it is evident from Fig. 35 the energy transfer from N_2 (X $^1\Sigma_g^+$) molecules to the lowest two CN (B $^2\Sigma^+$) vibrational levels is exothermic, thus this process will have a great efficiency even at low temperatures. On the other hand, this process is endothermic for higher CN (B $^2\Sigma^+$) vibrational levels,

thus its efficiency is lower. A resonance between N_2 ($X\ ^1\Sigma_g^+$, $v = 14$) and CN ($B\ ^2\Sigma^+$, $v = 2$) is slightly endothermic (–26 cm^{-1}). Due to this fact, this reaction can contribute to the population at the higher temperatures more significantly than at the lower temperatures. The reaction R19 competes with the main populating process of the N_2^+ ($B\ ^2\Sigma_u^+$) state.

Although the rate constant of reaction R19 is a little higher than for the reaction R14, the low temperature this rate constant is only 80 % of the value for the reaction R14. This could not explain why the CN violet emission replaces the nitrogen 1st negative emission during the pink afterglow. Also the radiative lifetime of the N_2^+ ($B\ ^2\Sigma_u^+$) states, which is about one half of that for the CN ($B\ ^2\Sigma^+$) state (30 ns [13], resp. 60 ns [28]) shows that the simple mechanism for the pink afterglow quenching could not be valid. The mechanism could be probably more complicated and the decrease of the nitrogen molecular ion production will play a significant role. This study is actually under preparation. The recombination of the C and N atoms described by the reaction R22 is indirect process as it was mentioned above. It is also possible to add the process R23 that has a high rate coefficient and it can be efficient at high atomic nitrogen concentrations.

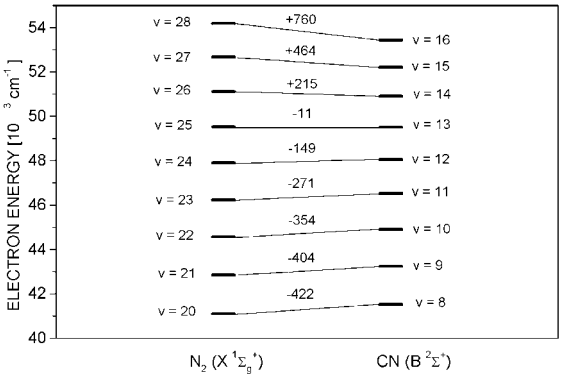

Fig. 37 Energy scheme of resonance vibrational energy transfer from N_2 ($X\ ^1\Sigma_g^+$) to higher levels of the CN ($B\ ^2\Sigma^+$) states

The transitions originated on high CN ($B\ ^2\Sigma^+$) vibrational levels are not observed very often at the laboratory conditions however many observations comes from the space observations. Due to the absence of appropriate data the model presented bellow can be used as the first estimation only. It can be supposed that the excitation energy transfer from the vibrationally excited nitrogen is the main process also in the population of these levels. Fig. 37 shows an energetic scheme illustrating this process. This figure is calculated for the following reaction:

$$N_2\ (X\ ^1\Sigma_g^+, v) + CN\ (X\ ^2\Sigma^+, v = 0) \rightarrow N_2\ (X\ ^1\Sigma_g^+, v = 0) + CN\ (B\ ^2\Sigma^+, v)$$

This reaction could not be the population mechanism for levels 10 and 11 due to the great negative energy balance but they can be populated by reactions with vibrationally excited CN ($X\ ^2\Sigma^+$) state. Similar process can contribute significantly to the population on the vibrational level 12, too. The reactions where the final N_2 ($X\ ^1\Sigma_g^+$) vibrational level is 1 are not probable.

Except this, probably main process, the energy transfer from lowest vibrational levels of the N_2 ($A\ ^3\Sigma_u^+$) state can contribute for highest levels populations [51], too. The contribution of the other processes like recombination or other processes are fully uncertain. To obtain any exact results about populating processes it will be necessary to prepare a new experiment using selectively excited nitrogen molecules.

9 CONCLUSION AND PERSPECTIVES

The study shows the complex experimental and theoretical description of the post-discharges in nitrogen and nitrogen–hydrocarbon mixtures. Some of the observations in pure nitrogen were made for the first time and the experiments using the mixtures of nitrogen with traces of hydrocarbons (including the halogenated) are original. The specific aim of the studies is the use of post-discharges at the temperature below the ambient. The main contributions of these studies to the human knowledge are in the verification of a strong influence of the nitrogen afterglow on the carbon traces and in the verification of many state specific reaction channels including the estimation of two reaction coefficients.

The study of the nitrogen post-discharge is not completed, of course. There are several promising directions for future research as pointed above. The possible directions are listed in the following summary.

- It is necessary to carry out the experiments in microwave and DC discharges on the same experimental set-up to compare the differences in kinetics of both afterglow types with respect to further applications.
- The processes in nitrogen–methane mixture can be used for the detection of disintegration of polymeric materials. The simple apparatus for this application was developed and it is necessary to verify its detection limits in the practice.
- It is probable that vibrationally excited nitrogen ground state molecules can during the collisions transfer their energy to the other species, not only to nitrogen, CN, and NO. Due to their high concentration in the post-discharge they can probably be used as an efficient excitation source for many molecular and atomic radiative states and thus the high intensity spectra of the other traces can be recorded and used in the field of analytic chemistry.
- It is necessary to test and specify the state specific reactions and their rate constants using the numerical kinetic models of the post-discharge. These models must be state-selective, so much more complex then simple models presented in this study.

The study of the post-discharges forms a wide field for experimental and theoretical studies. The four ideas above, of course, show only some of the possible directions for further research and they will be probably extended in the near future.

ACKNOWLEDGEMENTS

The special thanks must be done to the all colleges at all the laboratories. The initial impulses for the research presented in this volume originate from Prof. Jan Janča and from Assoc. Prof. Antonín Tálský, both from Masaryk University at Brno. Prof. André Ricard from France (actually at Toulouse) helped significantly at the interpretation of the experimental observations and also at preparation of the kinetic model. The author is grateful also for the technical staff at all the laboratories where the experimental work was provided. Without their collaboration the experiments could not be successfully finished. Author is indebted to Dr. Michal Křístek for linguistic corrections of this volume. The special thanks are reserved for Dr. Vít Kudrle who made the last correctors of this work. Studies presented in this volume were supported by the following grants and research programs:

- *Plasmachemical Processes in the Plasma and at Interface with Solids*, Grant Agency of Czech Republic, project 202/93/2118 (1993-1995).
- *Joint Laboratory for Applied Plasma Physics and Plasma Chemistry*, Complex Grant of Czech Ministry of Education, project VS 94 084 (1994-1998).
- *Etude des Réactions Cinétiques dans la Post-Décharge d'un Plasma Ar–N_2–CH_4*, Robert Schuman Foundation, France (1995-1996).
- *Study of the Processes in Plasma Created in Ar–N_2–CH_4 Gas Mixture*, Grant Agency of Academy of Science of Czech Republic, project C104 3601 (1996).
- *Studies of Plasmachemical Reaction Kinetics and Plasma Deposition Processes of Thin Layers on Solid Substrates*, Grant Agency of Czech Republic, project 202/96/0508 (1996-1998).
- *Hard and Ultra-hard Coatings Created by Non-conventional Plasma Processes*, Grant Agency of Czech Republic, project 106/96/K245 (1996-2000).
- *Study of the Processes in Post-discharge Plasma Created in Pure Nitrogen with Chloro- and Fluoro-Carbons and Their Application in Determination of the Plastic Materials Degradation*, Grant Agency of Czech Republic, project 202/98/P258 (1998-2001).
- *Homogeneous and Heterogeneous Materials on the Basis of Polymers and Biopolymers*, Czech Ministry of Education Research Layout, project CD MSM 263100019 (1998-2004).

REFERENCES

[1] Bachmann R., Li X., Ottinger Ch., Vilesov A. F., Wulfmayer V.: *J. Chem. Phys.* **98** (1993) 8606

[2] Becker K. H., Fink E. H., Groth W., Jud W., Kley D.: *Discuss. Faraday Soc.* **53** (1972) 35

[3] Belmonte T., Czerwiec T., Michel H.: *Surf. Coat. Technol.* **142** (2001) 306

[4] De Benedictis S., Dilecce G., Šimek M.: *Chem. Phys.* **178** (1993) 547

[5] Berkowitz J., Chupka W. A., Kistiakowsky G. B.: *J. Chem. Phys.* **25** (1956) 457

[6] Bolshakova L. G., Golubovskii Yu. B., Telezhko V. M., Stoyanov D. G.: *Sov. Phys. Tech. Phys.* **35** (1990) 665

[7] Brennen W., Shane E. C.: *J. Phys. Chem.* **75** (1971) 1552

[8] Carlson T. A., Duric N., Erman P., Larsson M.: *Phys. Scr.* **19** (1979) 25

[9] Cartwright D. C., Chutjian A., Trajmar S., Williams W.: *Phys. Rev. A* **16** (1977) 1013

[10] Cernogora G.: PhD. Thesis, University Paris-Sud, Orsay 1980

[11] Diamy A. M.: Private communications, Orsay 1994

[12] Gil T. J., Lengsfield B. H., Mc Curdy C. W., Rescigno T. N.: *Phys. Rev. A* **49** (1994) 2251

[13] Gilmore F. R., Laher R. R., Espy P. J.: *J. Phys. Chem. Ref. Data* **21** (1992) 1005

[14] Gordon E. B., Pelmenev A. A., Pugachev O. F., Khmelenko V.: *Chem. Phys.* **61** (1981) 35

[15] Guerra V., Loureiro J.: *Plasma Source Sci. Tech.* **8** (1999) 110

[16] Guerra V., Sa P. A., Loureiro J.: *J. Phys. D, Appl. Phys.* **34** (2001) 1745

[17] Herzberg G.: *Molecular Spectra and Molecular Structure, Vol. I: Spectra of Diatomic Molecules*, D. Van Nostrand Co., New York, 2nd ed., 1950

[18] Hochard L., Ricard A., Cernogora G.: *Proc. Conf.Planetologie*, Toulouse 1994

[19] Hubeňák J., Krčma F.: *J. Phys. D, Appl. Phys.* **33** (2000) 3121

[20] Ito H., Ozaki Y., Nagata T., Suzuki K., Kondow T., Kuchitsu K.: *Can. J. Phys.* **62** (1984) 1586

[21] Jackson W. M., Faris J. L.: *J. Chem. Phys.* **56** (1972) 95

[22] Janča J., Tálský A., El Kattan N.: *Folia Physica* **27** (1978) 23

[23] Janča J., Tálský A., Krčma F., Hochard L., Ricard A.: *Acta Phys. Univ. Comenianae* **35** (1995) 197

[24] Jaubertau J. L., Jaubertau I., Aubreton J.: *Chem. Phys. Lett.* **327** (2000) 351

[25] Katayama D. H., Dentamaro A. V., Welsh J. A.: *J. Chem. Phys.* **101** (1994) 9422

[26] Kley D., Washida N., Becker K. H., Groth W.: *Chem. Phys. Lett.* **15** (1972) 45

[27] Klopovsky K. S., Mukhovatova A. V., Popov A. M., Popov N. A., Popovicheva O. B., Rakhimova T. V.: *J. Phys. D, Appl. Phys.* **27** (1994) 1399

[28] Knowles P. J., Werner H. J., Hay P. J., Cartwright D. C.: *J. Chem. Phys.* **89** (1988) 7334

[29] Kovacs I.: *Rotational Structure in the Spectra of Diatomic Molecules*, Akadémiai Kiadó, Budapest 1969

[30] Krčma F.: *Spectroscopic Studies of the Methane Traces Influence on the Nitrogen Afterglow*, Thesis, Masaryk University, Brno 1995

[31] Krčma F.: Proc. SPPT XVIII, Praha 1997, 197

[32] Krčma F., Babák L.: Proc. ICPP XXV, Praha 1998, 2461

[33] Krčma F., Protasevich E. T.: *Post-discharges in Pure nitrogen and in Nitrogen Containing Halogenated Hydrocarbon Traces*, Tomsk Polytechnic University Publishing, Tomsk 2003

[34] Kumar V., Kumar A.: *Physica* **132 C** (1985) 273

[35] Legrand J. C., Diamy A. M., Hrach R., Hrachová V.: *Vacuum* **50** (1998) 491

[36] Levron D., Phelps A. V.: *J. Chem. Phys.* **69** (1978) 2260

[37] Li Z. Q., Zhou J. Y., Zhang J., Chen T. B., Yuan J.: *J. Alloy. Compd.* **346** (2002) 230

[38] Lofthus A., Krupenie P. H.: *J. Phys. Chem. Ref. Data* **6** (1977) 113

[39] Magne L., Cernogora G., Loureiro J., Ferreira C. M.: *J. Phys. D, Appl. Phys.* **24** (1991) 1758

[40] Marinelli W. J., Green B. D., DeFaccio M. A.: *J. Phys. Chem.* **92** (1988) 3429

[41] Markovič V. Lj., Pejovič M. M., Petrovič Z. Lj.: *J. Phys. D, Appl. Phys.* **27** (1994) 979

[42] De Monchy A. R.: *Nitrogen Afterglow*, Thesis, University Rotterdam, Rotterdam 1970
[43] Nestmann B. M., Pfingst K., Peyerimheff S. D.: *J. Phys. B* **27** (1994) 2297
[44] Oumghar A., Legrand J. C., Diamy A. M., Turillon N.: *Plasma Chem. Plasma Process.* **15** (1995) 87
[45] Ozaki Y., Ito H., Suzuki K., Kondow T., Kuchitsu K.: *Chem. Phys.* **80** (1983) 85
[46] Paniccia F., Gorse C., Cacciatore M., Capitelli M.: *J. Appl. Phys.* **61** (1987) 3123
[47] Partridge H., Langhoff S. R., Bauschlicher C. W.: *J. Chem. Phys.* **84** (1986) 6901
[48] Partridge H., Langhoff S. R., Bauschlicher C. W., Schwenke D. W.: *J. Chem. Phys.* **88** (1988) 3174
[49] Pearse R. W. B., Gaydon A. G.: *The Identification of Molecular Spectra*, fourth edition, London 1976
[50] Phelps A. V., Pitchford L. C.: Joint Institute for Laboratory Astrophysics Information, Report No. 26, 1985
[51] Pintassilgo C. D., Cernogora G., Loureiro J.: *Plasma Source Sci. Tech.* **10** (2001) 147
[52] Piper L. G.: *J. Chem. Phys.* **88** (1988) 231
[53] Piper L. G.: *J. Chem. Phys.* **88** (1988) 6911
[54] Piper L. G.: *J. Chem. Phys.* **91** (1989) 864
[55] Piper L. G.: *J. Chem. Phys.* **97** (1992) 270
[56] Piper L. G.: *J. Chem. Phys.* **101** (1994) 10229
[57] Pivovar A. V., Sidorova T. D.: *Sov. Phys. Tech. Phys.***30** (1985) 308
[58] Polak L. S., Sloveckii D. I., Sokolov A. S.: *Opt. Spectrosc.* **32** (1972) 247
[59] Polak L. S., Sergeev P. A., Slovetskii D. I.: *High Temp.* **15** (1977) 13
[60] Prasad C. V. V., Bernath P. F., Frum C., Engelman R.: *J. Mol. Spectrosc.* **151** (1992) 459
[61] Prasad C. V. V., Bernath P. F.: *J. Mol. Spectrosc.* **156** (1992) 327
[62] Ralston A. *Basis of Numerical Mathematics*, Academia, Praha 1978, 283-290 – in czech
[63] Rehfuss B. D., Suh M. H., Miller T. A., Bondybey V. E.: *J. Mol. Spectrosc.* **151** (1992) 437
[64] Ricard A., Tétreault J., Hubert J.: *J. Phys. B* **24** (1991) 1115
[65] Ricard A.: *Surf. Coat. Technol.* **59** (1993) 67
[66] Ricard A., De Souza A. R.: *J. Phys. III France* **4** (1994) 2593
[67] Ricard A., Cernogora G., Fitaire M., Hochard L., Kouassi N., Speller C., Vacher J. R.: *Planet. Space Sci.* **43** (1995) 41
[68] Sa P. A., Loureiro J.: *J. Phys. D, Appl. Phys.* **30** (1997) 2320
[69] Setser D. W., Thrush B. A.: *Proc. Roy. Soc. A* **288** (1965) 256
[70] Data Book 1990 *Siemens Optoelectronics*, Siemens AG, Munchen 1990, Part 8, 17
[71] Slovetskii D. I.: *Chemical Reaction Mechanisms in Non-equilibrium Plasma*, Nauka, Moscow 1980 - in russian
[72] Stedman D. H., Setser D. W.: *J. Chem. Phys.* **50** (1969) 2256
[73] Taïeb G., Legay F.: *Can. J. Phys.* **48** (1970) 1956
[74] Tanaka Y., Le Blanc F., Jursa A.: *J. Chem Phys.* **30** (1959) 1625
[75] Trajmar S., Register D. F., Chutjian A.: *Rep. Phys.* **97** (1983) 219
[76] Ung A. Y. M.: *J. Chem. Phys.* **65** (1976) 2987
[77] Ung A. Y. M.: *J. Chem. Phys.* **72** (1980) 3731
[78] Wang. J. J., Gillan E. G.: *Thin Solid Films* **422** (2002) 62
[79] Washida N., Kley D., Becker K. H., Groth W.: *J. Chem. Phys.* **63** (1975) 4230
[80] Werner H. J., Follomeg B.: *J. Chem. Phys.* **91** (1989) 5425
[81] Zipf E. C.: *Can. J. Chem.* **59** (1969) 1863